

INTERNATIONAL UNIVERSITY LIAISON INDONESIA

BACHELOR'S THESIS

**PERFORMANCE REVIEW AND ANALYSIS OF GUAV-190417
TARGET DRONE: CRUISING AND TURNING**

By

Raihan Syauqi

11201701011

Presented to the Faculty of Engineering
In Partial Fulfilment Of the Requirements for the Degree of

SARJANA TEKNIK

In

AVIATION ENGINEERING

FACULTY OF ENGINEERING

BSD City 15345

Indonesia

January 2021

APPROVAL PAGE

PERFORMANCE REVIEW AND ANALYSIS OF GUAV-190417 TARGET DRONE: CRUISING AND TURNING

RAIHAN SYAUQI

11201701011

Presented to the Faculty of Engineering
In Partial Fulfillment of the Requirements for the Degree of

SARJANA TEKNIK

In

AVIATION ENGINEERING

FACULTY OF ENGINEERING

Dr. Eng. Ressa Octavianty

Thesis Advisor

Date

Triwanto Simanjuntak, PhD

Thesis Co-Advisor

Date

Dr. Ir. Prianggada I Tanaya, MME

Dean of Faculty of Engineering

Date

EXAMINERS APPROVAL PAGE

Neno Ruseno, S.T., M.Sc

Examiner 1

Date

Dr. Ir. Erie Sandhita, M.Sc

Examiner 2

Date

Assoc. Prof. Chung-Yan Lin, PhD

Examiner 3

Date

Dr. Eng. Ressa Octavianty

Examiner 4

Date

Triwanto Simanjuntak, PhD

Examiner 5

Date

STATEMENT BY THE AUTHOR

I hereby declare that this submission is my own work and to the best of my knowledge, it contains no material previously published or written by another person, nor material which to a substantial extent has been accepted for the award of any other degree or diploma at any educational institution, except where due acknowledgment is made in the thesis.

Raihan Syauqi
Student

Date

ABSTRACT

Performance Review and Analysis of GUAV-190417 Target Drone: Cruising and
Turning

by

Raihan Syauqi

Dr. Eng. Ressa Octavianty, Advisor

Triwanto Simanjuntak, PhD, Co-advisor

In this thesis, the performance analysis of GUAV-190417 target drone was conducted, in particular during cruising and turning attitudes. The preliminary design and initial sizing of this UAV had been completed as part of a project of Aviation System Design course in International University Liaison Indonesia (IULI). Nevertheless, a preliminary analysis of its performances is needed before stepping into detail design and prototyping phases in order to meet the mission requirement and design objectives. In this study, the cruising and turning performances were carried out for various altitudes and load factor by assuming that the aircraft is in the steady-state condition. The aerodynamics characteristics, such as lift and drag coefficients (C_L and C_D) were estimated manually using Prandtl lifting line theory and validated by laminar simulation using OpenFOAM v8.0 software with values of $C_L = 0.3529$, and $C_L = 0.3826$ for theory and simulation, respectively. From the same computation, the parasite drag coefficient of this aircraft was approximately reached ~ 0.04 . The results showed that for cruising performance, the maximum range and endurance obtained at sea level for weight fraction 1.25 are 215 km and 90 minutes respectively. For the turning performance analysis at sea-level, the minimum turning radius and and turning time of 180° turn (T_π) were 66.07m and 3.73 s, respectively which tend to increase at higher altitude. Furthermore, the maximum values for bank angle ϕ and load factor n at sea-level is 80.96° and 6.36 respectively at an airspeed of 306.64 km/h. In addition, the values of ϕ and n in higher altitudes tend to reduce. It is also worth to mention that the weight fraction and load factor have a significant impact on the cruising and turning performance of this UAV target drone.

Keyword: *UAV, UAT, Target Drone, Range, Endurance, Turning Rate*

ACKNOWLEDGEMENTS

First and foremost, praises and thanks to Allah, the Almighty, for his showers of blessings throughout and upon the completion of my thesis.

I would like to express my sincere gratitude and appreciation for Dr. Ressa Octavianty, ST, M.Eng and Triwanto Simanjuntak, ST, M.Eng, PhD. whose consistent guidance, support, and encouragement has been invaluable throughout my thesis. Without them, the completion of my thesis would not have been possible.

I would like to acknowledge my colleagues from the Galaxy Target Drone team for allowing me to analyze the performance of the target drone. Also, special thanks to the following people: Faisal Tri Mulyawan, Jordan Yap Hong Yong, Mufti Akbar, Prana Rao, and Sonya Indrastuti. Your thoughtful comments and recommendations were vital. Thank you for putting up with me. Your generosity and patience are irreplaceable.

Lastly, I would like to thank my parents and my family, whose unconditional support and prayers gave me the confidence to successfully complete my studies.

Contents

Approval Page	i
Examiners Approval Page	ii
Statement by The Author	iii
Abstract	iv
Acknowledgements	v
Contents	vi
List of Figures	ix
List of Tables	xi
1 Introduction	1
1.1 UAV	1
1.2 Target Drones	2
1.3 UAV Market in Indonesia	2
1.4 Project Background	3
1.5 Aircraft Design	4
1.6 GUAV-190417 Target Drone	5
1.6.1 Conceptual Design	5
Design Benchmarking	5
Design Configuration	6
Material Selection	11
Airfoil Selection	12

	Electrical Components	13
	Payload	14
	Weight Estimation	16
	Draft Design	17
1.6.2	Preliminary Design	19
	Preliminary Sizing	19
	Airfoil Details	21
	Wing Details	22
	Engine Details	22
1.7	General Statement of Problem Area	23
1.8	Research Objectives	23
1.9	Research Scope	24
2	Literature Review	26
2.1	Equations of Motion	26
	2.1.1 Steady Straight Non Side-Slipping Flight	26
	2.1.2 Steady Non Side-Slipping Banked Turn	27
2.2	Aerodynamics Basis	29
	2.2.1 Basic Aerodynamic Requirements	29
	2.2.2 Parabolic Lift-Drag Polar	29
2.3	Cruising Performance	36
	2.3.1 Weight Fraction	36
	2.3.2 Range and Endurance	37
	2.3.3 Approximate Analytic Expression for Range and Endurance (Jet Propulsion)	40
2.4	Turning Performance	43
	2.4.1 Governing Equations	43
	2.4.2 Performance in a Coordinated Turn Equations	46
3	Research Methodology	49
3.1	Conceptual Design and Preliminary Sizing	49
3.2	Aerodynamics Review	51
3.3	Aerodynamics Profile Estimation	52
3.4	Parabolic Lift Drag Polar Estimation	53

3.5	Performance Estimation Using Excel	53
3.5.1	Cruising Performance Estimation	54
3.5.2	Turning Performance Estimation	55
4	Results and Discussions	56
4.1	Aerodynamics Analysis Using OpenFOAM	56
4.2	Cruising Performance	57
4.3	Turning Performance	58
5	Summary, Conclusion, Recommendation	65
5.1	Conclusion	65
5.2	Recommendation	67
	References	68
	Appendices	69
	Turnitin Report	70
	Curriculum Vitae	76

List of Figures

1.1	Aircraft design process	5
1.2	Various parametric comparison I.	7
1.3	Various parametric comparison II.	8
1.4	Design Factor Priorities	9
1.5	Airfoil series LS(1)-0417 plotted	12
1.6	C_l, C_d , and C_m at $Re = 6 \times 10^6$	13
1.7	Wiring diagram	14
1.8	AS-133 Miss distance indicator	15
1.9	The left figure represents the structure of GUAV-190417 and the right figure represents the Isometric view of GUAV-190417.	18
1.10	Top view, front view, and side view of GUAV-190417.	19
1.11	Wingspan sizing of GUAV-190417	20
1.12	Length and height sizing of GUAV-190417	20
1.13	Detailed wing dimensions	21
2.1	Forces acting upon steady non side-slipping banked turn	28
2.2	Elements of drag components	30
2.3	Parabolic lift-drag estimation of low-subsonic aircrafts	32
2.4	Maximum C_L/C_D value	35
2.5	Maximum lift-drag ratio	35
2.6	Mission nomenclature.	37
2.7	Determination of V/F and F for jet engine aircraft during constant altitude and engine control flight.	39
2.8	Range and endurance calculation.	39
2.9	Best range and endurance conditions in level flight for jet powered aircraft	42

2.10	True banked turn of a aircraft during steady level flight	44
2.11	Determining the turning radius of an aircraft.	47
3.1	Step-by-step process to determine the performance of GUAV-190417	50
3.2	Mesh topology of computational domain.	52
3.3	Performance Calculation Overview.	54
4.1	OpenFOAM results: Pressure distribution.	57
4.2	OpenFOAM results: relationship between C_L and C_D	58
4.3	OpenFOAM results: C_D at different iterations.	59
4.4	Range of GUAV-190417 using different weight fractions at different altitudes	60
4.5	Endurance of GUAV-190417 using different weight fractions	61
4.6	Drag at sea-level	61
4.7	Power required at sea-level	62
4.8	Radius of turn at different altitudes	63
4.9	Load factor and the airspeed at different altitudes	63
4.10	Load factor and the airspeed at different altitudes	64
4.11	Time required to make a 180° turn at different altitudes	64

List of Tables

1.1	Indonesian drone start-ups.	3
1.2	List and specification of existing of target drone.	6
1.3	Configuration 1: Cost optimized	7
1.4	Configuration 2: Weight focused	9
1.5	Configuration 3: Ideally producible	9
1.6	Configuration 4: Maximum performance	10
1.7	Configuration 5: Highly reliable	10
1.8	List of electrical components	13
1.9	Weight estimation	16
1.10	Dimension of GUAV-190417	21
1.11	Airfoil details of GUAV-190417	21
1.12	Wing details of GUAV-190417	22
1.13	Engine details for GUAV-190417	22
3.1	Meshes used in the simulation	52
4.1	C_L comparison between OpenFOAM and manual estimation.	56

List of Abbreviations

UAV	U n m anned A erial V ehicle
AoA	A ngle O f A ttack
CAD	C omputer A ided D esign
CFD	C omputational F luid D ynamics
COG	C enter O f G rav I ty
ECU	E ngine C ontrol U nit
ESC	E lectronic S peed C ontrol
FVM	F inite E lements M ethod
FOD	F oreign O bject D amage
ISA	I nternational S tandard A tmosphere
MDI	M iss D istance I ndicator
MTOW	M aximum T ake- O ff W eight
RPM	R otation P er M inute
UAT	U n m anned A erial T arget
UAV	U n m anned A erial V ehicle
UHF	U ltra H igh F requency
VDC	V olts D irect C urrent

PERFORMANCE REVIEW AND ANALYSIS OF GUAV-190417 TARGET DRONE:
CRUISING AND TURNING

Dedicated to my parents

CHAPTER 1

INTRODUCTION

1.1 UAV

Since the start of the 20th century, aircraft and aviation, by and large, have made significant advances, and most of them, because of military clashes. All through the past century, huge endeavors were made for the turn of events and improvement of UAVs. These powered airborne vehicles that don't convey human pilots, use the forces from aerodynamics to make it able to fly autonomously, remotely piloted from a distanced area, generate lift, and convey payloads. This automatically guarantees the safety of the operators from any harmful incidents that may occur and allowing them to conduct new tasks functionality which can increase the capability of each operation and optimize the capacity of the system (M. Sadraey, 2017).

UAVs are progressively being utilized in common flight, civil, and science research missions. The scope of applicability is tremendous to the point that they are utilized to complete missions in military aviation, including fire-ships and maritime drones that are commonly used in the navies for protection and destroy enemy ships remotely. Earlier in World Wars 1 and 2, airborne drones were commonly used as target practice for pilots. UAVs will keep on being applied in different military tasks because of their convenience in diminishing losses and empowering the execution of prominent and time-sensitive missions. Dominant UAV applications in military occasions includes: combat, reconnaissance and surveillance, logistics, search and rescue, and target and decoy(Valavanis, 2014).

UAV are categorized accordingly with respect to its size and purpose and each are given abbreviations as follows:

- HALE: High altitude long endurance

- MALE: Medium altitude long endurance
- TUAV: Medium range tactical UAV
- MAV : Micro UAV
- NAV : Nano-air vehicle

1.2 Target Drones

Originally, UAV models that were used during World War 1 were designed to carry and drop explosives to enemy targets using the preset controls. Since then, the time has found limited specialized warfare applications, such as gunnery drills, missile drills, or other simple payload missions. Given the advancing technologies in the defense department, new strategies and equipment are expected to carry out military training as efficient and productive as possible. These strategies and equipment training comprised of weapon testing, observations, and calibrations. One of the main technologies used in this department is the utilization of target drones.

Commonly known as Unmanned Aerial Target (UAT), target drones are usually used in the training of anti-aircraft crews, frequently look like a radio-controlled model airplane. More current drones may utilize radar, countermeasures, and comparable frameworks to emulate a manned aircraft. Asides from the shape of the body and its wing configuration, target drones varies from having a propeller or a jet engine, whether its launched by hand, a catapult or takes off like a normal aircraft, and the payload that it carries. These differences is what states the performance of the target drone such as the speed, altitude, range, and endurance.

1.3 UAV Market in Indonesia

Indonesia has been experimenting with drones since the early 2000's but the growth of the drone industry in Indonesia has surged ever since the ministry of industry established a road map to make "Indonesia 4.0". The drone manufacturers in Indonesia are divided into two, The existing establishments and the start-ups.

No.	Company	Purpose
1	MSMB	Agriculture
2	AgriMart	Agriculture
3	AgroDrone	Agriculture
4	Drone Spraying Indonesia	Agriculture
5	Motodoro UAV	Agriculture
6	TerraDrone	Inspection
7	AvirTech	Inspection
8	FotoUdara	Surveillance
9	AeroMap	Surveillance
10	Geomac	Multi-purpose remote sensing

TABLE 1.1: Indonesian drone start-ups.

The existing establishments such as PT Global Informasi Indonesia, PT Mandiri Muhibbah, PT Dirgantara Indonesia BPP Teknologi, and Lapan are much more experienced in drones compared to the listed startup companies in table 1.1 that have only appeared one by one since 2014.

1.4 Project Background

GUAV-190417, also known as Galaxy Target Drone got its name as the project itself started out in 2019 and utilized the LS-0417 airfoil. This research started on the 5th semester of the authors duration of study as a part of a project that is being developed for a course called System Design. Due to the surging demand over UAVs in various fields, the author was assigned in a group of 5 where they were tasked implement their skills and knowledge into a process of designing and modelling a UAV by setting its desired function, configurations, and size by integrating its conceptual and preliminary design to be able to create an actual prototype.

After analyzing the UAV market in Indonesia, the group decided on designing and building a target drone due to the following reasons:

- Currently, The Indonesian military acquires their target drones from Canada and Spain within an expensive price range, which is not cost efficient.

- The existing target drones are propeller target drones and are completely outdated, disabling the Indonesian military to compete in an international standard.

The main goal of the project was to develop a low-cost target drone that is powered by a jet engine and can be categorized as a qualified low-speed (subsonic) target drone. easy to build and maintain, and highly reliable to perform target and decoy missions. The main UAV specifications include:

- Equipped with a miss-distance indicator as its payload;
- Ability to reach a maximum velocity of 0.3 Mach;
- High strength and low weight structure;
- Long flight range and endurance;
- Good maneuverability.

The outcome of this project would benefit the group as they will be the first undergraduate students to develop a jet engine powered target drone in Indonesia. The Indonesian military would have domestic alternative when it comes to purchasing a target drone. The knowledge and skills obtained can be applied to motivate and educate people in Indonesia so that they can have the opportunity to control or mass produce a target drone.

Thus far, the group has passed the conceptual design phase and a portion of the preliminary design. A performance calculation and analysis at several crucial flight points are yet to be done. Among those crucial flight points are the cruising and turning performance.

1.5 Aircraft Design

The designing process of an aircraft is the step where engineers create and manufacture flying objects that satisfy the balance between the required specifications and characteristics. The main concerns in the designing process of the aircraft include the structure, weight, aerodynamics, performance requirements, stability and control of the aircraft, propulsion systems, communication systems, electronics

systems, aircraft payload to conduct certain operations, production, and cost of the aircraft manufacturing (M. H. Sadraey, 2012).

Figure 1.1 illustrates the processes that needs to be done when designing an aircraft. Firstly, benchmark studies need to be carried out and requirements are established to match the mission profile. Once requirements are specified and determined, the initial outer body of the aircraft can be then drafted, which is often known as the conceptual design phase . The next step is to conduct preliminary design, which is the most crucial step because advanced analysis of aerodynamics, structures, stability, control, and aircraft performances must be done. The preliminary design is then followed by a detailed design, which includes designing sub-parts of the aircraft which are ribs, spars, skins, and other subparts that are needed to manufacture the prototype. The production costs, production tasks, and bill of materials should also be considered during the preliminary and detailed design to successfully manufacture the prototype. When the prototype has been manufactured, the aircraft needs to be tested and analyzed to know whether it has fulfilled the mission profile.



FIGURE 1.1: Aircraft design process

1.6 GUAV-190417 Target Drone

1.6.1 Conceptual Design

In this design phase, it will deal with justifying the needs, identifying the potential roles, setting the operation criteria and drafting out the design of the target drone.

Design Benchmarking

There is an enormous wealth of data on civil aircraft, where hundreds of them are similar. They can be used to extract very useful statistics. In order to choose

PERFORMANCE REVIEW AND ANALYSIS OF GUAV-190417 TARGET DRONE:
CRUISING AND TURNING

parameters such as wing size, engine, (etc), it is crucial to carry out detailed simulations at the conceptual design stage and by using previous/existing statistical data, experience, or industrial espionage to set a benchmark that satisfies the mission profile of the target drone.

No.	Name of Target Drone	Empty weight kg	Max speed km/h	Thrust kN	Length m	Wingspan m	Endurance min
1	Banshee Jet 80	-	648	80	2.850	2.490	45.0
2	Banshee Jet 80+	-	720	90	2.850	2.490	45.0
3	DO-DT35	15,000	650	220	1.640	1.300	90.0
4	DO-DT25	30,000	450	320	2.950	2.550	80.0
5	BQM-34 Firebee	934,000	1190	-	6.900	3.900	115.0
6	BQM-74E	206,400	954	1100	4.000	1.800	68.0
7	BQM-74F	281,000	1110	-	4.500	2.100	120.0
8	Chuckar 3	123,000	972	1330	3.940	1.760	70.0
9	AVIC low speed	20,000	300	-	2.320	2.120	20.0
10	AVIC high speed	-	1000	-	4.050	1.800	60.0
11	Argus As 292	27,000	100	2200	2.400	2.400	30.0
12	Denel Dynamics Skua	-	1062	-	6.000	3.570	85.0
13	Lavochkin La-17	-	900	-	8.440	7.500	60.0
14	GTD-Kilat	21,000	160	185	1.847	2.300	45.0
15	SCRAB 2	90,000	432	-	2.940	2.520	60.0
16	SCRAB 3	140,000	7200	-	3.130	2.000	60.0

TABLE 1.2: List and specification of existing of target drone.

As seen on table 1.2, the missing variables notated with a (-) were due to the limited information provided by the manufacturers on their websites. However, from this table itself, relations such as length to empty weight, length to thrust, wingspan to empty weight, and wingspan to thrust shown in Figures 1.2 and 1.3 could be made for comparison purposes.

Design Configuration

Before coming up with aircraft configurations, aircraft designers must set design factor priorities. These priorities depends on the mission profile such as the performance and reliability and the manufacturing conditions such as the build cost and producibility of the aircraft. For this project, the design factor priorities are set as shown in Figure 1.4.

Once the design factor priorities are determined, the next step is to come up with configurations that suits the design factor priorities best. The following configurations from Tables 1.3 to 1.7 were made to satisfy each design factors.

PERFORMANCE REVIEW AND ANALYSIS OF GUAV-190417 TARGET DRONE:
 CRUISING AND TURNING

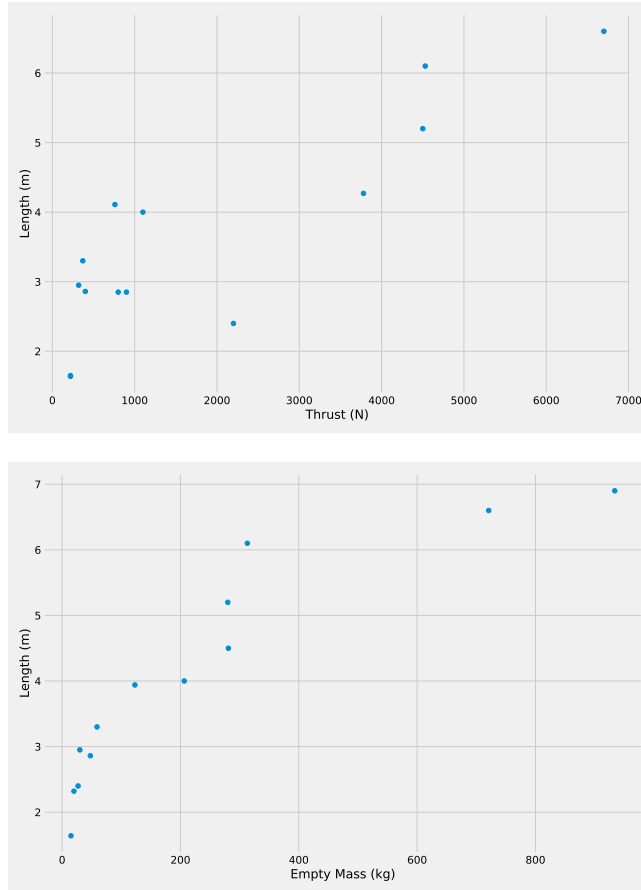


FIGURE 1.2: Various parametric comparison I.

Body	BWB
Wing type	Compound
Wing position	Middle
Braking system	Hydraulic disc brakes
Landing gear	Single main
Engine position	Wing
Airsurface controller	Elevon without rudder
Canard	No
Vertical stabilizer	Single

TABLE 1.3: Configuration 1: Cost optimized

PERFORMANCE REVIEW AND ANALYSIS OF GUAV-190417 TARGET DRONE:
CRUISING AND TURNING

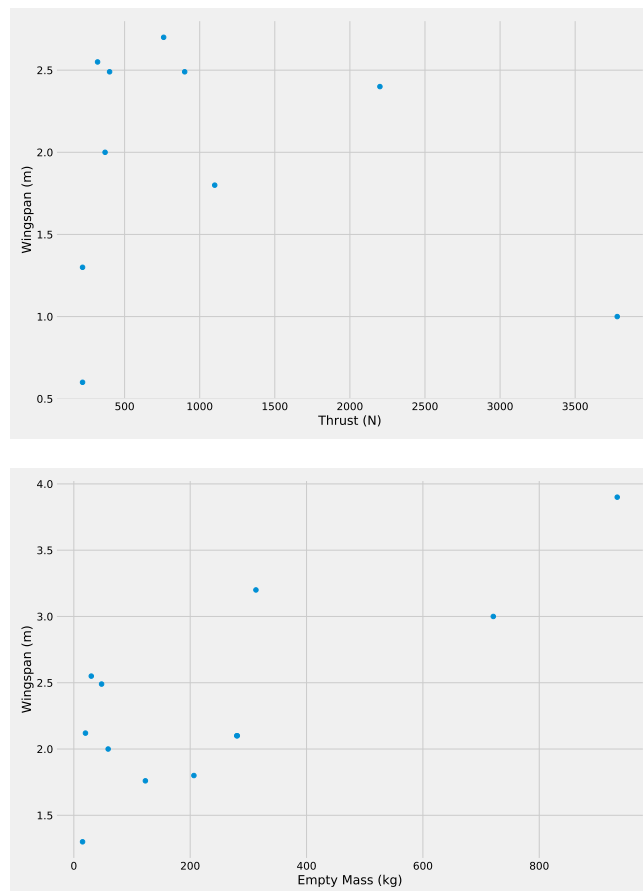


FIGURE 1.3: Various parametric comparison II.

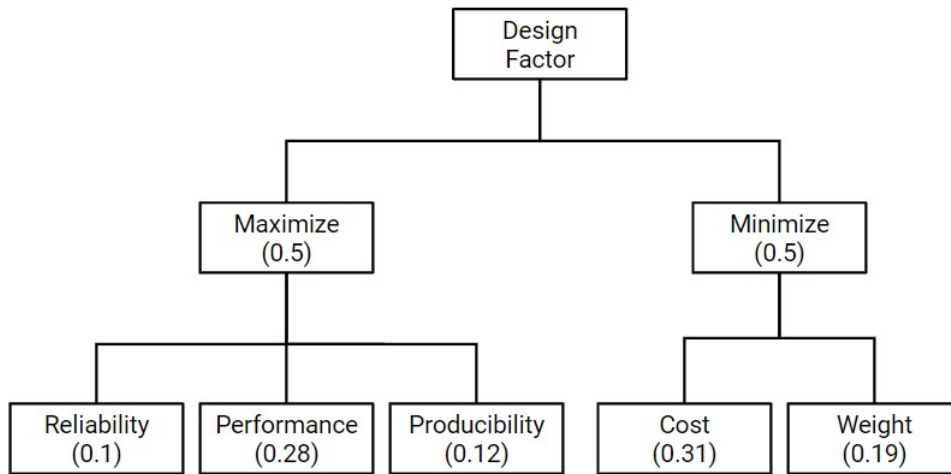


FIGURE 1.4: Design Factor Priorities

Body	BWB
Wing type	Tailed
Wing position	Middle
Braking system	Electromagnetic disc brakes
Landing gear	Single main
Engine position	Tail / rear
Airsurface controller	Elevon without rudder
Canard	No
Vertical stabilizer	Single

TABLE 1.4: Configuration 2: Weight focused

Body	Conventional
Wing type	Tailed
Wing position	Middle
Braking system	Electromagnetic disc brakes
Landing gear	Single main
Engine position	Tail / rear
Airsurface controller	Elevon with rudder
Canard	No
Vertical stabilizer	Single

TABLE 1.5: Configuration 3: Ideally producible

Body	Conventional aircraft body
Wing type	Lambda delta
Wing position	Middle
Braking system	Electromagnetic disc brakes
Landing gear	Multi bogey
Engine position	Tail / rear
Airsurface controller	Primary control surface
Canard	Yes
Vertical stabilizer	Double

TABLE 1.6: Configuration 4: Maximum performance

Body	Conventional aircraft body
Wing type	Cropped
Wing position	Middle
Braking system	Electromagnetic disc brakes
Landing gear	Quadricycle
Engine position	Tail / rear
Airsurface controller	Primary control surface
Canard	No
Vertical stabilizer	Double

TABLE 1.7: Configuration 5: Highly reliable

Out of the five configurations made, it has been finalized that configuration 3 is the one that fits best within the desired design factors and the mission profile for this project. Despite being ideally producible, the components chosen for configuration 3 can impact the performance of the target drone. The advantage and disadvantages are listed as shown below:

- Advantages:
 1. Swept back wing operates better on low speeds and are much more stable at high α .
 2. Tricycle landing gear are stable during ground maneuver and only requires a shorter takeoff run.
 3. Electromagnetic disc brakes has a high degree in safety.
 4. Middle wing position are more streamlined.

5. Tail/ rear engine positions has lower risk of FOD.
 6. Primary control surface are user friendly making it easy to control the drone.
 7. Utilizing only 1 vertical stabilizer results in less induced drag.
- Disadvantages:
 1. Swept back wing has high tip drag and can roll out of control when yawing.
 2. Tricycle landing gears are highly complex.
 3. Electromagnetic disc brakes uses electric power to brake.
 4. Middle wing position aircraft's are harder to land.
 5. Tail/ rear engine positions strengthens the fuselage which adds more weight.
 6. Primary control surface involves more moving parts.
 7. Utilizing only 1 vertical stabilizer results in reduced stress on the root.

Material Selection

Other than cost and availability of a material, the weight of the GUAV-190417 is an important design factor. Other than being light the drone must be able to withstand all the forces experienced. Hence why the suitable material is classified to have a high strength to weight ratio. Stiffness of the material is also crucial as it would be imprudent for the GUAV-190417 to deform tremendously during operation. Lastly, the effect of corrosion is a serious matter when it comes to deciding the materials of an aircraft as corrosion would likely be able to degrade the material strength and may cause failures to the aircraft.

Balsa wood is suitable due to the high strength to weight ratio. Other than the fact that it is obtainable and inexpensive, it is also easy to fabricate. The relatively low density of balsa wood gives an advantage as it allows the aircraft to glide and have high maneuverability. However, balsa wood has got a relatively low stiffness compared to other materials. When subjected to high concentration load, balsa wood tends to easily undergo plastic deformation. Therefore, to protect the

aircraft structure from breaking apart, two layers of fiberglass should be coated on the aircraft using resin to make it firm. Once the fiberglass and resin is applied, a layer of glazing compound is applied to smoothen and level the texture of the structure. Lastly, a final layer of paint is applied to prevent the aircraft from corrosion due due water exposure or extreme conditions.

Airfoil Selection

The cross-section of an aircraft's wing is known as the airfoil. Aerodynamic forces are produced when an airfoil-shaped body moving through fluid produces. Choosing the correct airfoil is very crucial as each airfoil is designated for different flight purposes. The right airfoil determines the speed of flight, the amount of that the wing will be able to generate the desired lift and drag, and at what point the aircraft stalls. However, airfoil profile has a vital effect on the aircraft performance and should be selected carefully.

During airfoil selection process, other than non aerodynamic characteristics such as section thickness to minimize the structural weight and provide enough storage for fuel, and undercarriage, the main characteristics sought after are high maximum lift, low drag, low pitching moment, and specific stall behavior. These characteristics all depends on the mission profile of the aircraft which will have direct impact to the aerodynamics and the performance of an aircraft (McGhee, 1980).

Considering the mission profile of GUAV-190417, the most suitable airfoil is the LS-0417 MOD. The airfoil shape and characteristics are shown in the following Figures 1.5 and 1.6.

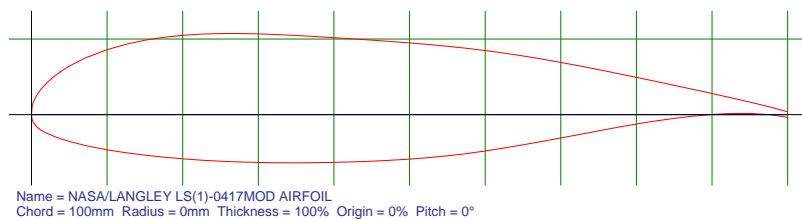


FIGURE 1.5: Airfoil series LS(1)-0417 plotted

PERFORMANCE REVIEW AND ANALYSIS OF GUAV-190417 TARGET DRONE:
CRUISING AND TURNING

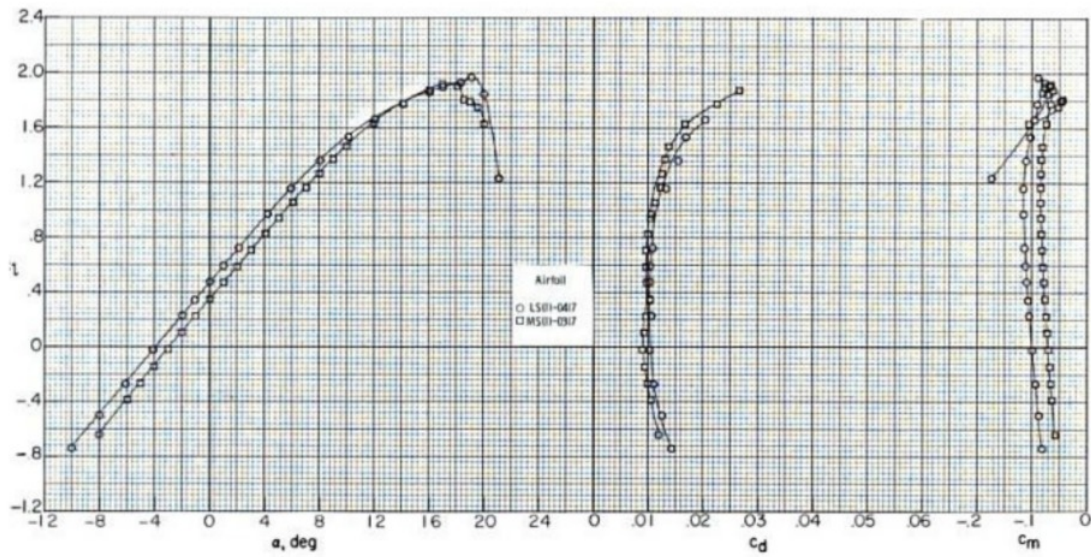


FIGURE 1.6: C_l, C_d , and C_m at $Re = 6 \times 10^6$

Electrical Components

There are 5 major electrical components that are required to operate the aircraft to meet and satisfy its mission profile requirements. Table 1.8 shows the detailed list of electrical components along with its type and specification.

No	Component	Type	Specification
1	Transmitter	RadioLink AT9/ AT9S	10 Channels Control distance: Ground 900 meters, Air 3400 Support receiver: R9DS, R12DS, R12DSM, R6D6, R6DSM
2	Receiver	RadioLink R9D	9 Channels PWM signals Working voltage: 4.8V to 10V Working current: 38mA to 45mA Input voltage: 5V Dimension: 43mm x 24mm x 15mm Weight:10.7g
3	Servo	Emax Servo Metal Gear Digital FEETECH FT5316M	Operating angle: 180° Operating speed: 0.18s/ 60° (4.8V) 0.16s/ 60° (6V) Stall torque: 14.3kg to 15.5kg Dimension: 40mm x 20.2mm x 38mm Weight: 56g
4	Li-Po battery	Baterai Turnigy Nano-tech 2200 mAh 3s 35c Lipo Pack	Capacity: 2200mAh Voltage: 3S1P/ 3 Cell/ 11.1 V Weight: 199g (including wire, plug, and case) Dimensions: 115mm x 35mm x 27mm
5	IC	IC 7809	Input voltage range: above 11.5V Current rating I_c : 1A Output voltage range: 9V

TABLE 1.8: List of electrical components

Electrical components in an aircraft needs to be wired and placed properly in a way that it would function. The listed electrical components in table 1.8 should

be wired down as shown in the wiring diagram in Figure 1.7.

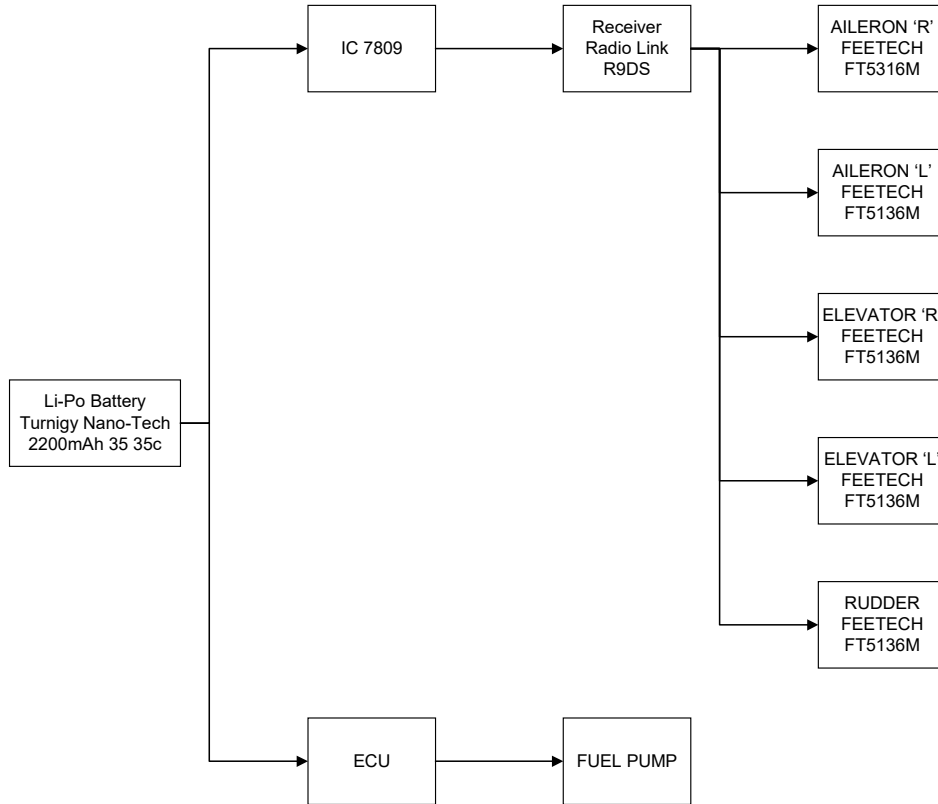


FIGURE 1.7: Wiring diagram

Payload

One of the most essential part when conducting retraining and retesting operations of the aircraft is by performing a miss distance indicator (MDI). The MDI is a universal type and there are many MDI platforms that are able to be integrated into any kinds of towed aerial target. The MDI is able to handle all kinds of target courses relating to missiles including passing courses and attacking, while also presenting real-time results of the missile to the user. The missed distance is determined by the amplitude of the shock wave and the angular position is determined by the sequence of blows between different indicator pressure sensors. As mentioned, the missed distance and angular position of the missiles will be

measured in real-time and the data is transferred through the specially designed VHF/UHF transmitter as raw data signals to the scoring system. This MDI system measures the miss distance between a missile or a burst of gunfire and a target vehicle, which is a remotely piloted target drone. The missed distance is described as the minimum separation between the two bodies. The distance is obtained from a post-processing analysis of the encounter images received from the two trackers, and triangulation is used to obtain the relative trajectories of the missile and the target vehicle.

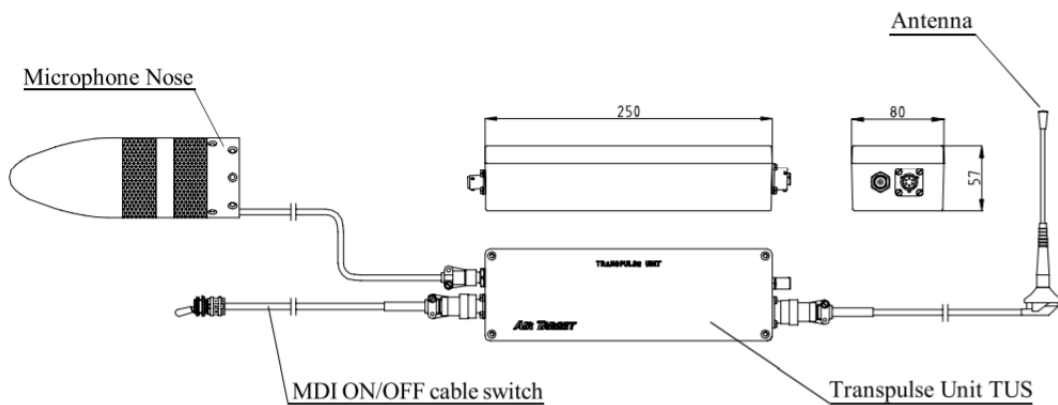


FIGURE 1.8: AS-133 Miss distance indicator

As shown in figure 1.8, provided by Air Target Sweden, the AS-133 is an universal 12-sector MDI which is most suitable for the mission profile of the target drone. The A-133 is intended to to be installed in the nose of both hard targets and target drones/ UAV's. Weighing approximately 2 kg, the A-133 MDI consists of 4 main components:

- A microphone nose containing six pressure sensors
- A cylindrical body containing the electronics
- A transmitter
- A rechargeable NIMH accumulator

The rechargeable NIMH accumulator enables the MDI to operate actively for a minimum of 4 hours at +24°C utilizing a 12 VDC supply voltage. With 6 selectable ranges in sensitivity, these components enables the system to accumulate 6000 rounds per minute, momentarily more, in terms of scoring capacity with scoring calibers of 12.7 mm to 5"+ and missiles. It is capable of reading results of min ±1m or ±15% of the actual miss distance, whichever is the greatest at angular accuracy of ±15°.

Weight Estimation

No.	Component	Weight (kg)
1	Engine	5.00
2	Fuel	8.00
3	Fuel tank	0.40
4	Body	12.00
	Wing	
	Elevon	
	Vertical stabilizers	
5	Brakes	0.10
6	Landing gear	0.50
7	Wires	0.02
8	Servo	0.20
9	MDI	2.00
Estimate weight		28.22
Additional weight		6.78
Total weight estimation		35.00

TABLE 1.9: Weight estimation

Table 1.9 shows the breakdown of the weight of the GUAV-190417 is estimated and shown in table above. The total weight of the drone is estimated by adding up the total weight of all the existing components that would be used. To account for alterations or developments to the drone, an additional 6.78kg of weight is added. Therefore, the total estimated weight is $28.22\text{kg} + 6.78\text{kg} = 35\text{kg}$.

Draft Design

The primary elements of the GUAV-190417 airframe are the fuselage, wing, and tail section. Most airframes consist of main structural component types, including spars, ribs, and skin. The spar is known to be the main structural component of the wing that runs throughout the spanwise at right angles to the fuselage. The spar carries flight loads and the weight of the wings to bear forces such as spanwise bending and transverse shear loads. The ribs of the wing are made of balsa structures that are powered by the spar, capable of carrying plane loads that are positioned wisely along the length of the wing.

Other than operating in re-distributing loads, the wings ribs also hold the skin with the designed contour shapes. The ribs of the wings are also capable of reducing the effective buckling length which results in an increase in the compressive load capability. In order to reach an efficient torsion member, a layer of skin is applied to cover the wings. A relatively thin layer of skin is used in many air vehicles that travel at subsonic speeds, designed specifically so that they can sustain post-buckling. Therefore, it can be assumed that the thin layer of skin is not considered in making any contribution to the bending of the wing, where the bending moment is taken up by the spars.

The GUAV-190417 is also intended to allow the disassembly and exchanging of parts. This target drone is designed to be able to be separated into modular units. The modular units are known as the ability to disintegrate the aircraft so that it is able to generate smaller components. This accommodates the ease in parts replacement, while also promoting easy maintenance, transportation, and testing. They are:

1. 1x Fuselage
2. 2x Wing
3. 2x Horizontal stabilizer
4. 1x Vertical stabilizer
5. 1x Engine mount
6. 1x Jet engine

Utilizing SolidEdge software, a CAD model was created to build the design of the target drone. The target drone along with its structure is shown in figure 1.9.

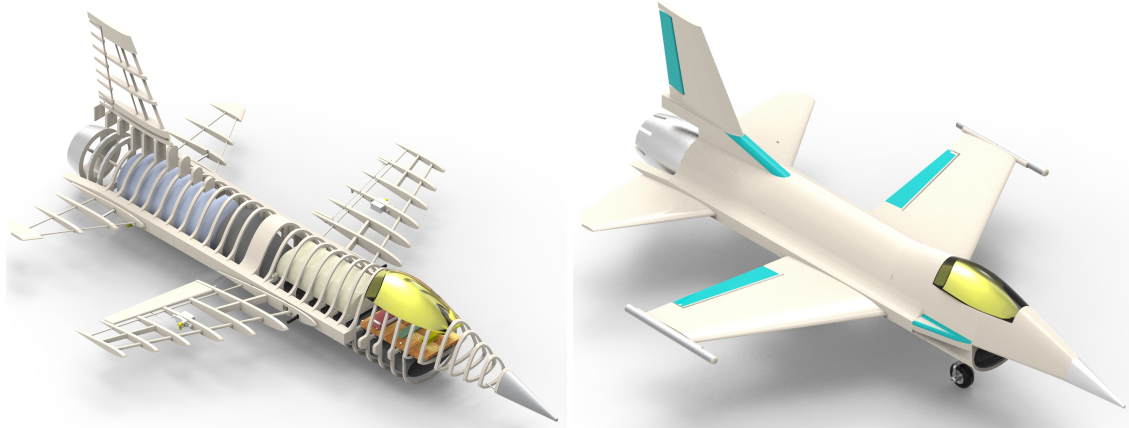


FIGURE 1.9: The left figure represents the structure of GUAV-190417 and the right figure represents the Isometric view of GUAV-190417.

Although target drones are considered as air vehicles, the major difference between the structures and materials of a target drone and other engineering structures and materials lies in their weight. The main objective of the design of this target drone is to reduce weight and at the same time be strong enough to withstand the forces acting on it during flight. Therefore, most materials used for a medium-scale target drone aircraft are required to have a high strength to the weight ratio in order for it to be considered suitable for target drone aircraft applications.

The GUAV-190417 structure is designed to ensure that every piece of material is used to its full potential. This can be achieved by using airframe structures, where numerous parts are joined and assembled together as a whole. Illustrated in figure 1.10, most of the aircraft part's size and shape are determined based on their non-structural considerations, hence why these airframe structures are required to maintain the shape of the design. For this reason, the target drone is designed by also considering the dimensions of the components required, availability, and weight of these various components.



FIGURE 1.10: Top view, front view, and side view of GUAV-190417.

1.6.2 Preliminary Design

In this design phase, it will deal with working on the selection, specifications, and limitations of the target drone.

Preliminary Sizing

In this section, as shown in figures 1.11, 1.12, 1.13 the dimensions of the target drone is specified. The dimensions are also listed in Table 1.10 when is the foundation of carrying out the preliminary design. Without specifying the length, width (wingspan), and height of the target drone, the aerodynamics and performance calculations will not be possible (Roskam, 1986).

PERFORMANCE REVIEW AND ANALYSIS OF GUAV-190417 TARGET DRONE:
CRUISING AND TURNING

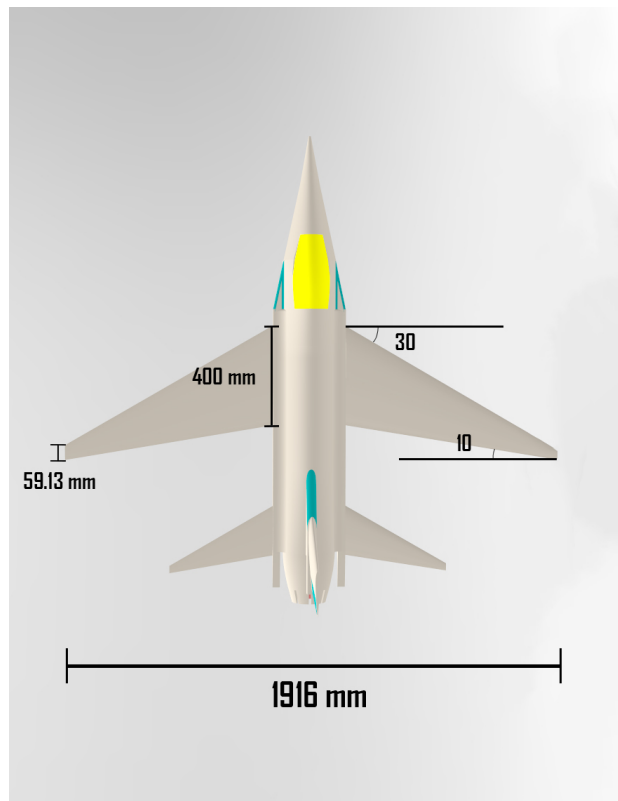


FIGURE 1.11: Wingspan sizing of GUAV-190417

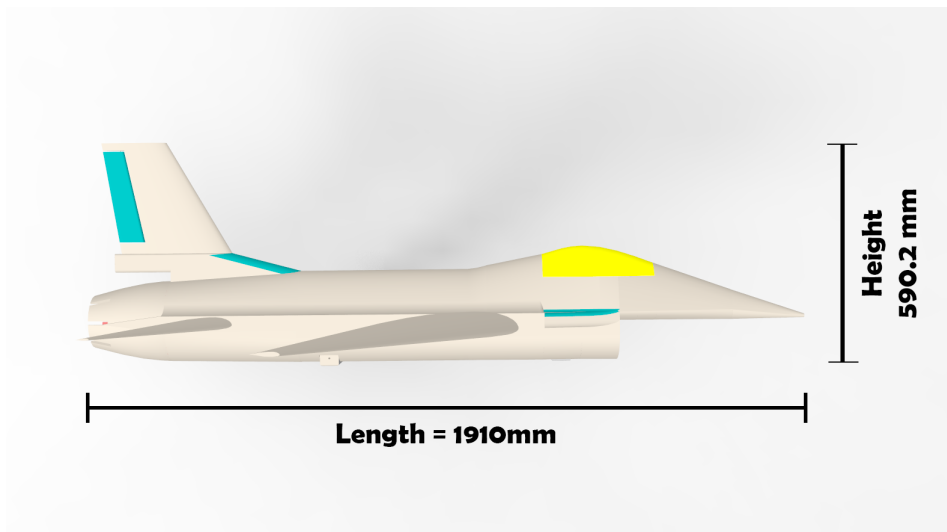


FIGURE 1.12: Length and height sizing of GUAV-190417

Dimension	Value (mm)
Length	1910.00
Height	590.20
Wingspan	1916.00

TABLE 1.10: Dimension of GUAV-190417

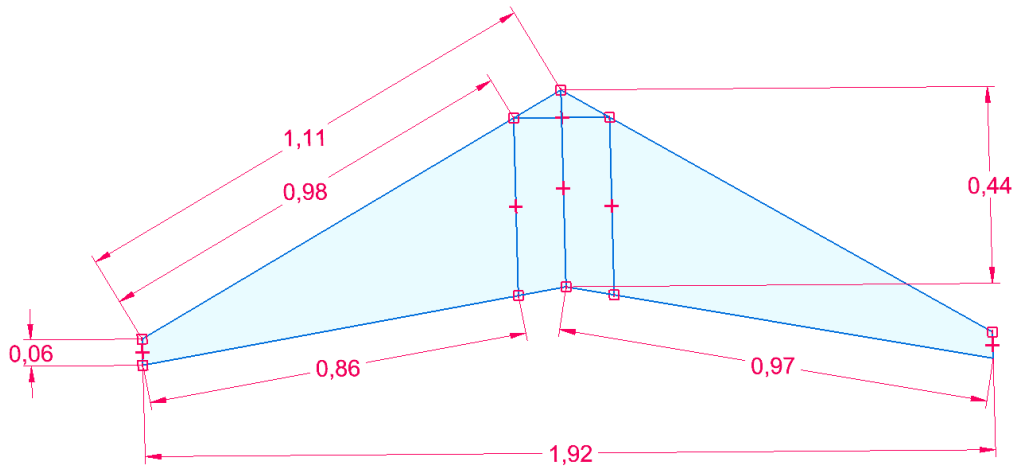


FIGURE 1.13: Detailed wing dimensions

Airfoil Details

The details from this section can be seen on table 1.11

Airfoil Characteristics	Result
Max airfoil thickness	0.17 c
$\alpha_{c_{l=0}}$	-4°
c_{l_α}	0.3814 /rad
c_{m_α} for $\alpha > 6^\circ$	0.2455 /rad
c_{m_α} for $\alpha < 4^\circ$	-0.1705 /rad
$\alpha_{c_{l_{\max}}}$	17°
$c_{l_{\max}}$	1.95

TABLE 1.11: Airfoil details of GUAV-190417

Wing Details

The details from this section can be seen on table 1.12.

Wing characteristics	Result
Wingspan	1.916 m
Chord at root	0.059 13 m
Chord at tip	0.578 75 m
Taper ratio	0.102 17
Lower swept angle	30°
Upper swept angle	10°
Swept angle mean to mean	20.85°
Gross area	0.481 35 m^2
AR	7.627
C_L	0.109 24
C_D	0.072 66
C_{D_i}	0.000 77
C_{D_0}	0.040 00
θ	6.237 61
$C_L/C_{D_{\max}}$	9.60
$C_L^3/C_{D_{\max}}^2$	96.65
$C_L/C_{D_{\max}}^2$	148.52

TABLE 1.12: Wing details of GUAV-190417

Engine Details

The details from this section can be seen on table 1.13.

Engine specification	Result
Mach	0.3
Velocity	103.2 m/s
Weight	343 N
Rho	1.225 kg/m^3
Thrust max	250 N
C_T	0.000 444 284 1/s
Viscosity	0.000 017 89 kg/m/s

TABLE 1.13: Engine details for GUAV-190417

1.7 General Statement of Problem Area

With an existing conceptual and preliminary design data of GUAV-190417, the design would not be able to be reviewed and would not be eligible to move on to the next process of creating a detailed design and prototype manufacturing without carrying out a performance analysis. Focusing of cruising and turning performance, the knowledge of the requisite aircraft cruising and turning characteristics is essential to assess whether if an aircraft successfully satisfies its given mission profile. The need to understand the maximum range, endurance, turning radius, and rate of turn along with the required velocity and forces needed to accomplish a certain mission at specific altitudes cannot be understated as it would give an overview whether if the aircraft is optimum or not. The availability of fuel for a jet engine UAV is limited. Therefore, the characteristics of the target drone and the environment that impacts the maximum range and endurance must be distinguished. These information are pivotal when it comes to the marketing of the target drone.

1.8 Research Objectives

The objectives of this research are to investigate:

- The parabolic lift drag polar using OpenFOAM, whether if it is similar to the parabolic lift drag polar calculated manually.
- The weight fraction of GUAV-190417 at cruising mission segment.
- The range, endurance, and average velocity of GUAV-190417 at different altitudes.
- The load factor at different bank angles for turning performance.
- The velocity, drag, power required, radius of turn, and rate of turn of GUAV-190417 at different altitudes.

1.9 Research Scope

- Only the cruising and turning performance is discussed in this thesis. The airfield, symmetric climbing, and gliding performance has been distinguished. (Yong, 2021)
- Non standard atmospheric conditions or weather phenomena which impacts the performance of the target drone are not taken into consideration.
- Since the estimated weight may differ in reality once the target drone is manufactured, the performance will have an effect with respect to the actual weight of the target drone.
- The reliability of analytical aerodynamic estimation, formulas, and relationships may be limited as the research and analysis followed were obtained from established literature. $(C_L/C_D)_{max}$ is not subjected to the altitude but rather on the aerodynamic design boundaries; e , AR , and C_{Do} of the aircraft. The $(C_L/C_D)_{max}$ cannot occur at a specific velocity and the velocity at which C_L/C_D is obtained does not alter with altitude.
- The engine related data required such as T and SFC were obtained from a group of colleagues who were tasked to design and manufacture a subsonic jet engine. The data gathered were obtained by measuring and reading off related curves. Human error may contribute to the inaccuracy of data.
- For cruising performance, a steady straight non-sideslipping, unaccelerated flight profile is assumed in estimating the range and endurance, enabling the ease of drag analysis. However, it does not reflect on the reality as the target drone could be flying with some sideslip at certain cruising phase of the flight. In order to account for the change in each individual drag profile would be a tedious process, hence why the assumption was made
- For turning performance, a steady level non-sideslipping bank turn flight profile in estimating the turning radius and rate of turn at different bank angles. The power available is assumed to always be sufficient to the power required. The thrust available is assumed to be sufficient to overcome the

drag which neglects the drag equation in the longitudinal set of equations, which ignores the drag trim.

- Taking the time frame for the completion of this research into account, the quality of the thesis may be directly or indirectly affected.

CHAPTER 2

LITERATURE REVIEW

The most important requirement for a new UAV design is that it fulfills its mission profile. This is assured through performance calculations at the design stage. Performance calculations are crucial at several flight points. Among those crucial flight points are cruising and turning performance.

2.1 Equations of Motion

2.1.1 Steady Straight Non Side-Slipping Flight

To have a better understanding of aircraft performances, there are four main forces that are acting on the aircraft, which are:

1. Lift
2. Drag
3. Thrust
4. Weight

The performance calculations and analysis done within this thesis are under the parameters of steady acceleration and altitude, also known as static performance. The term static performance is referred to the performance of an aircraft where their flight conditions are unaccelerated. The static performance analysis leads to reasonable calculations of maximum velocity, maximum range, and even parameters of vital interest of aircraft design and operation.

Level flight means that the flight path is along the horizontal, which is $\theta=0$. Since unaccelerated flight means that the right sides of these equations are equal to zero. Thus, establishing equations that can be simplified as:

$$T \cos \alpha_T = D \quad (2.1)$$

$$L + T \sin \alpha_T = W \quad (2.2)$$

For most conventional aircraft, α_T is small and insignificant enough that $\cos \alpha_T \approx 1$ and $\sin \alpha_T \approx 0$. Hence equations :

$$T = D \quad (2.3)$$

$$L = W \quad (2.4)$$

These equations are the equations of motion for level and unaccelerated flight. In a level and unaccelerated flight, the aerodynamic drag is balanced by the engine thrust, and the aerodynamic lift is balanced by the aircraft weight.

2.1.2 Steady Non Side-Slipping Banked Turn

The relationship between the angle of bank ϕ , aerodynamic angle of roll μ , and the flight-path angle γ is represented by:

$$\sin \phi = \sin \mu \cos \gamma \quad (2.5)$$

As shown in figure 2.1, due to the non-existing sideslip, the side force S equals to zero (0) so that the aerodynamic resultant force occurs on the plane of symmetry. Therefore, the vector of the sum of the weight W and the centrifugal force C also lies in the same plane of symmetry. The equilibrium equations are given by:

$$\begin{aligned} T \cos \alpha_T - D - W \sin \gamma &= 0 \\ W \cos \gamma \sin \mu - C \cos \mu &= 0 \\ -T \sin \alpha_T - L + W \cos \gamma \cos \mu + C \sin \mu &= 0 \end{aligned} \quad (2.6)$$

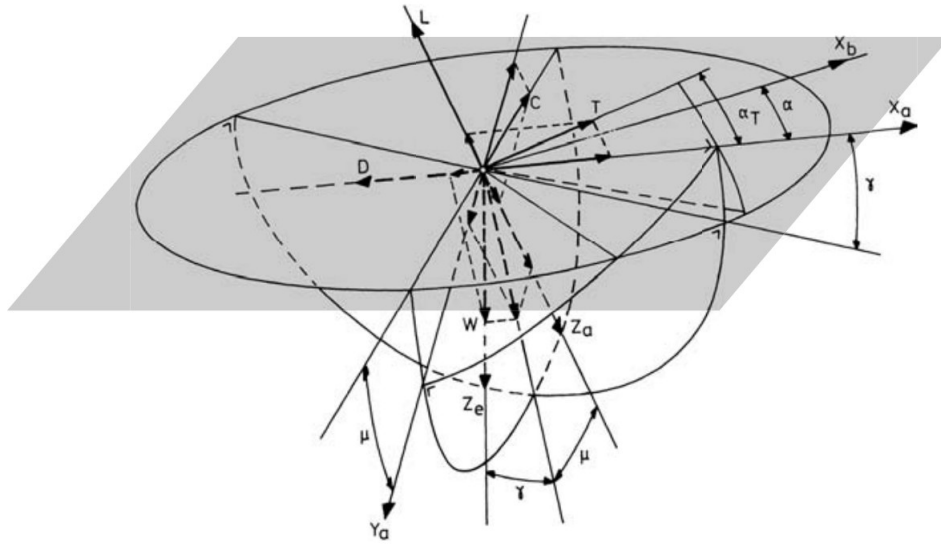


FIGURE 2.1: Forces acting upon steady non side-slipping banked turn

The second equation represents that in a coordinated turn, the components of the centrifugal force along the Y_a -axis are balanced completely by a lateral component of the weight of the airplane.

$$\begin{aligned}
 T \cos \alpha_T - D - W \sin \gamma &= 0 \\
 -T \sin \alpha_T \sin \mu + L \sin \mu - C &= 0 \\
 -\sin \alpha_T \cos \mu - L \cos \mu + W \cos \gamma &= 0
 \end{aligned} \tag{2.7}$$

The first equation represents the equilibrium of forces along the X_a -axis. The second equation represents the summation of the radial forces in the horizontal plane. The third equation represents the summation of the forces that are acting perpendicular to the X_a -axis in the vertical plane.

2.2 Aerodynamics Basis

2.2.1 Basic Aerodynamic Requirements

The values from the wing sizing and the airfoil characteristics of an aircraft contributes to the aerodynamics characteristics of an aircraft. Hence why it has a vital effect on the aircraft performance(Anderson Jr, 2010).

These aerodynamics characteristics comprises of the aspect ratio, Oswald efficiency number, constant k, Reynold's number, and taper ratio. The equations for the characteristics are listed respectively

$$AR = \frac{b^2}{S} \quad (2.8)$$

$$e = 4.61(1 - 0.045AR^{0.68})[\cos(\Lambda_L E)]^{0.15} - 3.1 \quad (2.9)$$

$$k = \frac{1}{\pi A R e} \quad (2.10)$$

$$Re = \frac{\rho V S}{\mu} \quad (2.11)$$

$$\text{Taper Ratio} = \frac{C_t}{C_r} \quad (2.12)$$

2.2.2 Parabolic Lift-Drag Polar

The total drag of a plane can be segmented into the drag of the wing D_W and the amount of the components D_n :

$$D = D_W + D_n \quad (2.13)$$

As shown in figure 2.2, the wing drag composes as the amount of the induced drag D_i and the profile drag D_p . Hence the equation can be formed as:

$$D = D_i + D_p + D_n \quad (2.14)$$

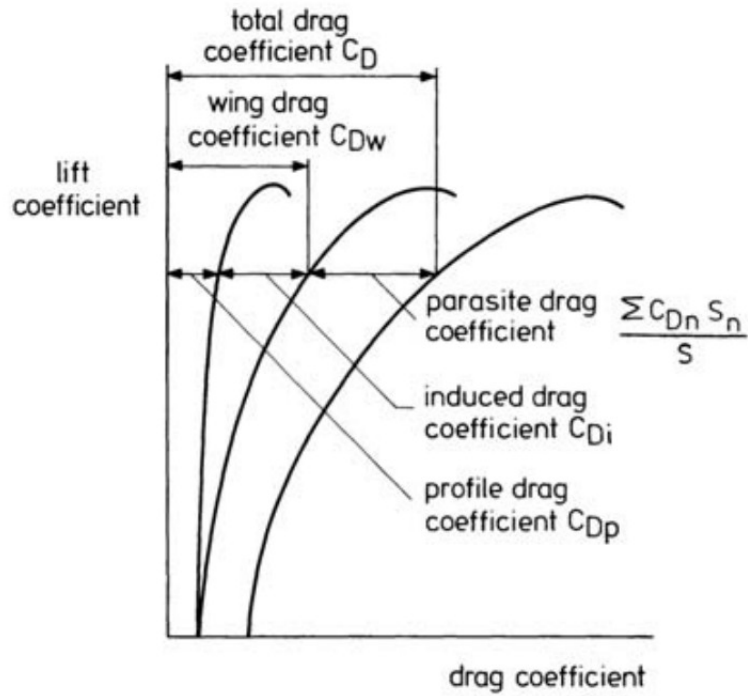


FIGURE 2.2: Elements of drag components

The profile drag comprises pressure drag, skin friction drag, and wave drag. The wave drag is zero for subsonic velocities beneath the critical Mach number. Pressure drag, skin contact drag and wave drag together, form the drag of the aircraft components. Since the drag coefficient of each component part, C_{Dn} , is based on a certain area S_n as the reference area, the total aircraft drag is given as:

$$C_D \frac{1}{2} \rho V^2 S = C_{Di} \frac{1}{2} V^2 \rho S + C_{Dp} \frac{1}{2} V^2 \rho S + (\sum C_{Dn} S_n) \frac{1}{2} \rho V^2 \quad (2.15)$$

The above equation for total drag of the aircraft can be simplified by eliminating the common variables from both sides to form:

$$C_D = C_{Di} + C_{Dp} + \frac{\sum C_{Dn} S_n}{S} \quad (2.16)$$

Since the drag coefficient of each component part, C_{Dn} , is based on a certain area S_n as the reference area, the total aircraft drag is given. Hypothetical stream-lined features predicts that the induced drag coefficient is straightforwardly relative

to the square of the lift coefficient C_L , and contrarily corresponding to the angle proportion Λ and a wing effectiveness factor ϕ . The factor ϕ relies principally upon the wing planform since it demonstrates how close the elliptic spanwise lift conveyance is acquired. For an elliptic lift circulation $\phi = 1$ (least initiated drag coefficient). In any remaining cases ϕ will be short of what one. Hence, the drag coefficient of the plane is

$$C_D = \frac{C_L^2}{\pi AR\phi} + C_{Dp} + \frac{\Sigma C_{Dn} S_n}{S} \quad (2.17)$$

Since additionally, the profile drag and parasite drag coefficients are reliant on the angle of attack, the equation can be composed as:

$$C_D = \frac{C_L^2}{\pi AR\phi} + XC_L^2 + \left[C_{Dp} + \frac{\Sigma C_{Dn} S_n}{S} \right]_{C_L=0} \quad (2.18)$$

The variables within the parenthesis can be calculated to find zero lift drag coefficient, also known as C_{Do} . The variables XC_L^2 is the assumed parabolic change of the profile drag and the parasite drag due to its lift coefficient. Hence, The equation can be modified as:

$$C_D = C_{Do} + \frac{C_L^2}{\pi AR e} \quad (2.19)$$

Where the factor e , also known as Oswald's proficiency factor, represents the variety of the profile and parasite drag coefficients with lift coefficient, and the impact of the genuine spanwise lift distribution on induced drag coefficient. For most aircraft types, the estimation of e differs somewhere in the range of 0.6 and 0.9 (Anderson Jr, 2010).

$$\frac{1}{e} = X\pi AR + \frac{1}{\phi} \quad (2.20)$$

In some cases, the k factor which can be calculated as $1/(\pi AR e)$, also known as induced drag factor, can be used to simplify the equation above as:

$$C_D = C_{Do} + kC_L^2 \quad (2.21)$$

o

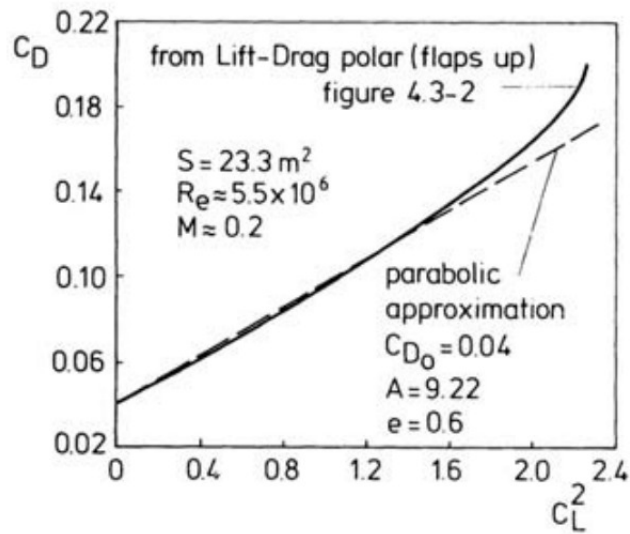


FIGURE 2.3: Parabolic lift-drag estimation of low-subsonic aircrafts

From figure 2.3, the deviation from the parabolic form is portrayed by the difference from the straight (specked) line. We see that an extensive piece of the lift-drag polar is undoubtedly a parabola, yet there is some additional drag at lift coefficients past about 1.0. The illustrative lift-drag polar can be utilized at subsonic velocities. Additionally, at both transonic and supersonic velocities, the estimations of C_{D0} and k are changed suitably. It might here be noticed that in numerous regards, the aircraft performance are dictated by the accompanying aerodynamic ratios: C_L/C_D , C_L^3/C_D^2 and C_L/C_D^2 . Noted that the maximum values of these ratios are crucial. For maximum C_L/C_D , the ratios can be separated with regards to C_L and set the main derivative equivalent to zero.

When it comes to finding the $(C_L/C_D)_{max}$, the final formula can be derived from

$$\begin{aligned}
 \frac{d(C_L/C_D)}{dC_L} &= 0 \\
 \frac{\frac{dC_D}{dC_L}C_D - C_L \frac{dC_D}{dC_L}}{C_D^2} &= 0 \\
 C_D - C_L \frac{dC_D}{dC_L} &= 0 \\
 C_D &= C_L \frac{dC_D}{dC_L} \\
 \frac{dC_D}{dC_L} &= \frac{C_D}{C_L}
 \end{aligned} \tag{2.22}$$

Where

$$\begin{aligned}
 C_D &= C_{D0} + kC_L^2 \\
 C_D &= C_{D0} + \frac{C_L^2}{\pi A Re} \\
 \frac{dC_D}{dC_L} &= 0 + \frac{2C_L}{\pi A Re}
 \end{aligned} \tag{2.23}$$

Using the substitution method for equation 2.22 and equation 2.23, C_L can be obtained as

$$\begin{aligned}
 \frac{C_D}{C_L} &= \frac{2C_L}{\pi A Re} \\
 2C_L^2 &= \pi A Re C_D \\
 2C_L^2 &= \pi A Re (C_{D0} + \frac{C_L^2}{\pi A Re}) \\
 2C_L^2 &= \pi A Re C_{D0} + C_L^2 \\
 C_L^2 &= \pi A Re C_{D0} \\
 C_L &= \sqrt{\pi A Re C_{D0}}
 \end{aligned} \tag{2.24}$$

Using the insertion method for equation 2.24 into equation 2.20, C_D can be obtained as

$$\begin{aligned}
 C_D &= C_{D0} + \frac{(\sqrt{\pi A Re C_{D0}^2})}{\pi A Re} \\
 C_D &= C_{D0} + C_{D0} \\
 C_D &= 2C_{D0}
 \end{aligned} \tag{2.25}$$

Finally, using the substitution method from equation 2.24 and equation 2.25, $(C_L/C_D)_{max}$ can be obtained as

$$\begin{aligned}
 \left(\frac{C_L}{C_D}\right)_{max} &= \frac{C_L}{C_D} \\
 &= \frac{\sqrt{\pi A Re C_{D0}^2}}{2C_{D0}} \\
 &= \frac{1}{2} \frac{\pi A Re}{C_{D0}}
 \end{aligned} \tag{2.26}$$

Figure ?? and ?? illustrates the point where maximum C_L/C_D and the maximum lift drag polar ratio can be achieved.

When it comes to finding the maximum value of C_L^3/C_D^2 , it can be obtained by differentiating it with respect to C_L and equating it to zero. The final formula can be derived from

$$\frac{dC_D}{dC_L} = \frac{3C_D}{2C_L} \tag{2.27}$$

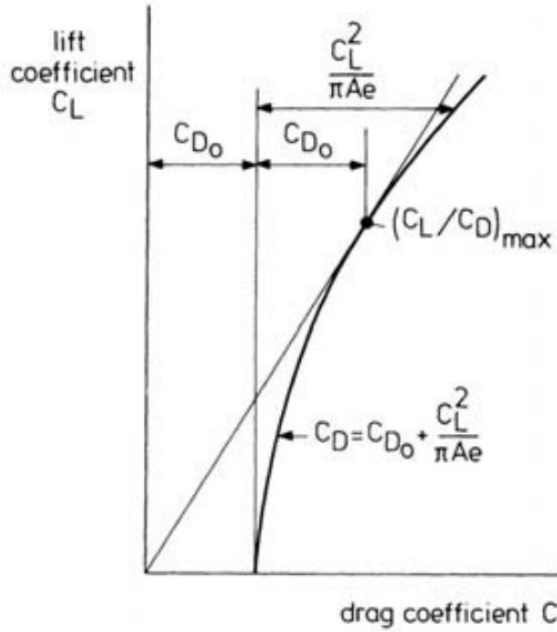
Differentiate C_D with respect to C_L to get

$$\frac{dC_D}{dC_L} = \frac{2C_L}{\pi A Re} \tag{2.28}$$

Using the substitution method for equation 2.27 and equation 2.28, C_L can be obtained as

$$c_L = \sqrt{3C_{D0}\pi A Re} \tag{2.29}$$

Using the substitution method for equation 2.29 and equation 2.20, C_D can be obtained as



elmaxclcd1

FIGURE 2.4: Maximum C_L/C_D value

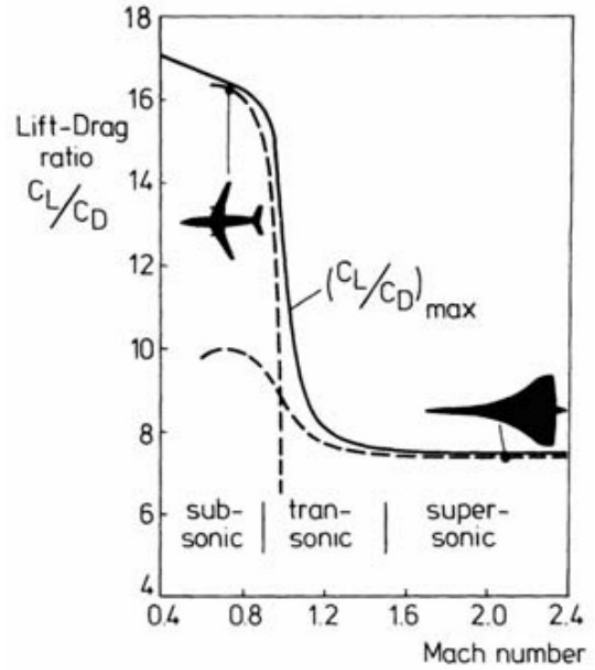


FIGURE 2.5: Maximum lift-drag ratio

$$C_D = 4C_{D0} \quad (2.30)$$

Finally, using the substitution method from equation 2.29 and equation 2.30, $(C_L^3/C_D^2)_{max}$ can be obtained as

$$\frac{C_L^3}{C_D^2} max = \frac{3\sqrt{3}}{16} \pi A R e \sqrt{\frac{\pi A R e}{C_{D0}}} \quad (2.31)$$

When it comes to finding the $(C_L/C_D^2)_{max}$, it can be obtained by differentiating it with respect to C_L and equating it to zero. The final formula can be derived from

$$\frac{dC_D}{dC_L} = \frac{C_D}{2C_L} \quad (2.32)$$

Differentiate C_D with respect to C_L to get

$$\frac{dC_D}{dC_L} = \frac{2C_L}{\pi A Re} \quad (2.33)$$

Using the substitution method for equation 2.32 and equation 2.33, C_L can be obtained as

$$C_L = \sqrt{\frac{C_D o \pi A Re}{3}} \quad (2.34)$$

Using the substitution method for equation 2.34 and equation 2.20, C_D can be obtained as

$$C_D = \frac{4C_D o}{3} \quad (2.35)$$

Finally, using the substitution method from equation 2.34 and equation 2.35, $(C_L/C_D^2)_{max}$ can be obtained as

$$(C_L/C_D^2)_{max} = \frac{3\sqrt{3}}{16} \sqrt{\frac{\pi A Re}{C_D o^2}} \quad (2.36)$$

Be advised that the maximum lift-to-drag ratio $(C_L/C_D)_{max}$ is a significant aerodynamic quantity of an aircraft.

2.3 Cruising Performance

A cruise can be defined as a flying state in which the aircraft uses the most economically efficient fuel and optimally designed technical conditions. This phase has the longest air trip duration and has a mission to arrive at the designated destination. During the cruise state, the condition of the speed and altitude of the aircraft movement are both relatively constant.

2.3.1 Weight Fraction

Weight fraction of an aircraft can simply be defined as W_1/W_2 where W_1 is the MTOW and W_2 is $(MTOW - W_{fuel})$. However, when taking the mission segments of an aircraft into consideration, the weight fraction can be redefined as the fuel

gets burnt during flight phases up to the point where weight fraction is desired to calculate the performance of an aircraft.

For the case of calculating cruising performance, the aircraft has to undergo engine start and warm-up, taxi, take-off, and climbing and acceleration until it reaches the cruising phase. The weight fraction for different flight phases are listed below (Raymer, 2012):

- Engine start, taxi, and take-off: 0.970
- Climbing and acceleration: 0.985
- Cruising: 0.995

2.3.2 Range and Endurance

From figure 2.6, range represents the distance traveled by the aircraft in a horizontal straight line of a cruising flight. In the other hand, the distance traversed in a climbing, cruising, and descending flight is often known as total range, stage length, or a block distance (Ruijgrok, 2009).

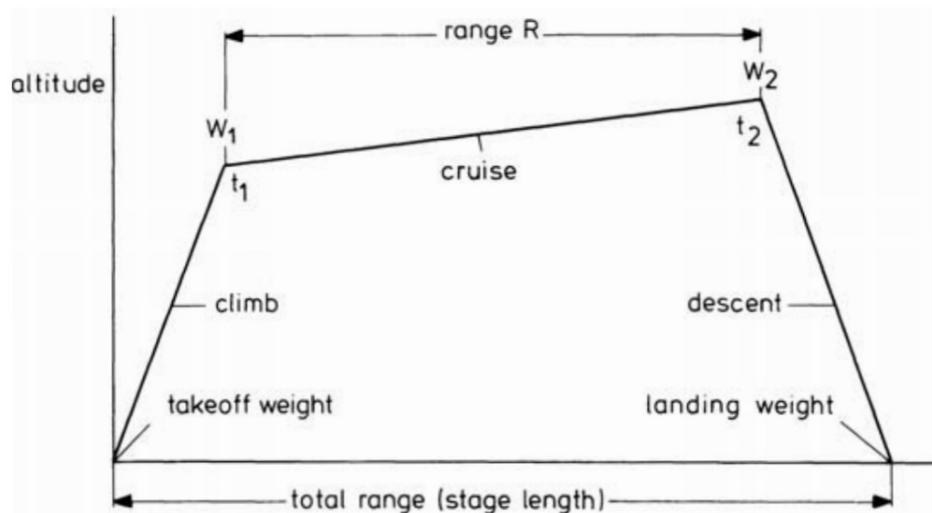


FIGURE 2.6: Mission nomenclature.

To acquire the maximum total range of an aircraft, fuel consumption per unit time has to be calculated as maximum total range can be defined as the distance an aircraft can fly between takeoff and landing limited by its fuel capacity.

$$F = \frac{dW_f}{dt} \quad (2.37)$$

W_f is noted as the total fuel load. The fuel weight flow rate is related to the weight of the aircraft. Since $dW_f = -dW$, equation 2.37 can be rewritten as

$$F = \frac{dW}{dt} \quad (2.38)$$

From the following definite integral, range can be distinguished as

$$R = \int_{t_1}^{t_2} V dt = \int_{W_1}^{W_2} -\frac{V}{F} dW = \int_{W_2}^{W_1} dW \quad (2.39)$$

Where V/F is the range per unit fuel weight (specific range)

Endurance is defined as the length of time spent in cruising flight. From the following definite integral, endurance can be distinguished as

$$E = \int_{t_1}^{t_2} dt = \int_{W_1}^{W_2} -\frac{dW}{F} = \int_{W_2}^{W_1} \frac{dW}{F} \quad (2.40)$$

At this point it is important to remember that in symmetric flight, the time history of the flight condition depends on the specification of two control laws, that is to say, the description of the variation of two control variables with time. Generally, both control variables are held constant throughout the cruise so that the flight condition only changes due to the influence of fuel consumption on the weight of the aircraft (M. H. Sadraey, 2017).

From figure 2.7, it can be distinguished that for jet engine aircraft, fuel flow rates can be obtained from the following equation

$$F = C_T T \quad (2.41)$$

Where C_T is the specific fuel consumption and T is thrust.

By looking at figure 2.8, it can be said that once the range and the endurance of an aircraft is determined, the average airspeed (V_{avg}) can be found by the following formula

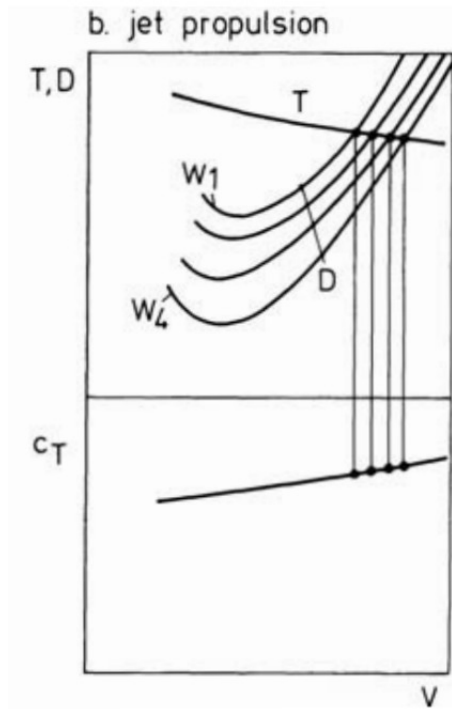


FIGURE 2.7: Determination of V/F and F for jet engine aircraft during constant altitude and engine control flight.

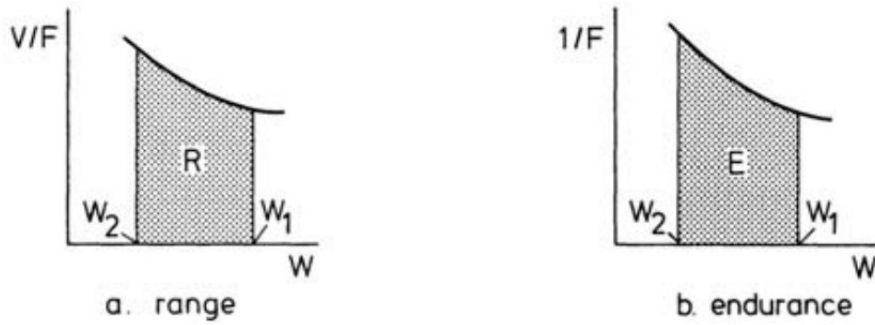


FIGURE 2.8: Range and endurance calculation.

$$V_{avg} = \frac{Range}{Endurance} \quad (2.42)$$

2.3.3 Approximate Analytic Expression for Range and Endurance (Jet Propulsion)

Using the relationship of drag

$$D = \frac{C_D}{C_L}W \quad (2.43)$$

The thrust can be distinguished as

$$T = D = \frac{C_D}{C_L}W \quad (2.44)$$

Using the relationship of airspeed

$$V = \sqrt{\frac{W}{S} \frac{2}{\rho} \frac{1}{C_L}} \quad (2.45)$$

Using the substitution method for equation 2.45 and equation 2.39, range can be distinguished as

$$R = \int_{W_2}^{W_1} \frac{1}{C_T W} \sqrt{\frac{W}{S} \frac{2}{\rho} \frac{1}{C_L}} dW \quad (2.46)$$

Using the insertion method for equation 2.44 and equation 2.41 into equation 2.40, endurance can be distinguished as

$$E = \int_{W_2}^{W_1} \frac{1}{C_T} \frac{C_L}{C_D} \frac{dW}{W} \quad (2.47)$$

In deriving analytic expressions for range and endurance, first, we shall consider cruising at a fixed height and at a constant angle of attack. Moreover, we shall continue to assume that the specific fuel consumption remains constant for the duration of the flight.

The analysis will be further simplified by neglecting the variation of the effects of compressibility on the aerodynamic characteristics of the aircraft as the flight speed reduces during the course of the flight. Integrating equation 2.46, range can be distinguished as

$$\begin{aligned}
 R &= \frac{1}{C_T} \sqrt{\frac{2 C_L}{S \rho C_D^2}} \int_{W_2}^{W_1} \frac{dW}{\sqrt{W}} \\
 &= \frac{2}{C_T} \sqrt{\frac{2 C_L}{S \rho C_D^2}} \left| \sqrt{W} \right|_{W_2}^{W_1} \\
 &= \frac{2}{C_T} \sqrt{\frac{2 C_L}{S \rho C_D^2}} [\sqrt{W_1} - \sqrt{W_2}]
 \end{aligned} \tag{2.48}$$

Noted that since $\sqrt{\rho}$ is present, its is crucial for jet powered aircrafts to have high cruising altitudes. Hence, equation 2.48 can be rewritten as

$$\begin{aligned}
 R &= \frac{2}{C_T} \sqrt{\frac{W_1 2 C_L}{S \rho C_D^2}} \left[1 - \sqrt{\frac{W_2}{W_1}} \right] \\
 &= 2 \frac{V_1 C_L}{C_T C_D} \left[1 - \sqrt{\frac{W_2}{W_1}} \right]
 \end{aligned} \tag{2.49}$$

Noted that V_1 is the initial airspeed, by integrating equation 2.47, endurance can be distinguished as

$$\begin{aligned}
 E &= \int_{W_2}^{W_1} \frac{1}{C_T} \frac{C_L}{C_D} \frac{dW}{W} \\
 &= \frac{1}{C_T} \frac{C_L}{C_D} \left| \ln W \right|_{W_2}^{W_1} \\
 &= \frac{1}{C_T} \frac{C_L}{C_D} \ln \frac{W_1}{W_2}
 \end{aligned} \tag{2.50}$$

A cruise technique of interest for turbojet and turbofan aircraft is the flight at constant airspeed and angle of attack. The flight-path angle occurring in this cruise-climb schedule, however, is normally sufficiently small so as to approve the use of the level-flight conditions that lift is equal to weight and thrust is equal to drag. Assuming that C_T and $\frac{C_L}{C_D}$ have constant values throughout the flight, range and endurance can directly be distinguished as

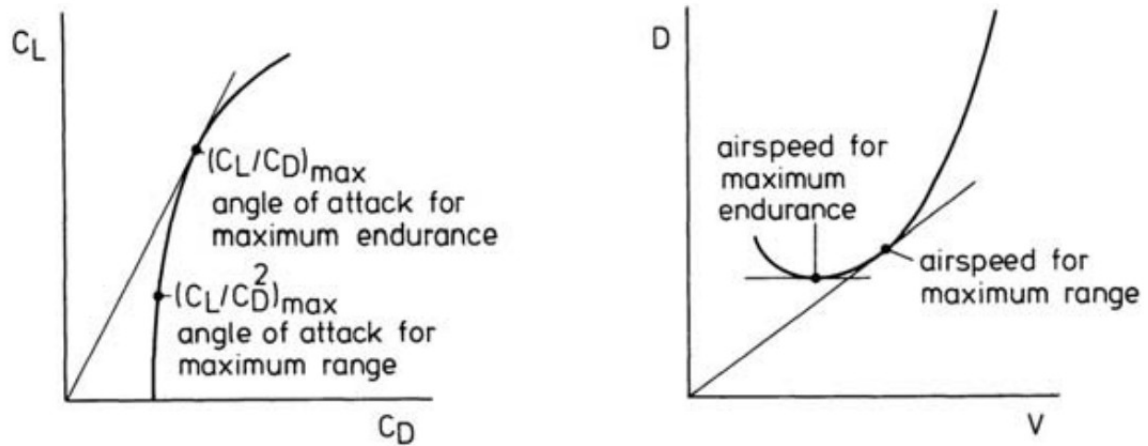


FIGURE 2.9: Best range and endurance conditions in level flight for jet powered aircraft

$$R = \frac{V}{C_T} \frac{C_L}{C_D} \ln \frac{W_1}{W_2} \quad (2.51)$$

$$E = \frac{R}{V} = \frac{1}{C_T} \frac{C_L}{C_D} \ln \frac{W_1}{W_2} \quad (2.52)$$

The quantity of $\frac{V}{C_T} \frac{C_L}{C_D}$ is known as the range factor. The greatest endurance can be found when $\frac{C_L}{C_D}$ is maximum.

Also, by assuming that C_T and $\frac{C_L}{C_D}$ have constant values throughout the flight, the range does not have an absolute maximum. Due to the absence of compressibility drag, a constrained optimum is obtained when the airspeed is specified. For this state, maximum range occurs at maximum C_L/C_D . This case requires the height at which the minimum drag speed becomes equivalent to the desired airspeed. With the condition of constant speed of sound at lower stratosphere for cruise-climb flight, a fixed airspeed relates to a fixed flight Mach number. This results in the constant aerodynamics ratio in equation 2.51

Referring to the thrust equation

$$T = C_D \frac{1}{2} \rho V^2 S \quad (2.53)$$

Where V is

$$V = \sqrt{\frac{W}{S} \frac{2}{\rho} \frac{1}{C_L}} \quad (2.54)$$

It can be elaborated that the thrust is directly proportional to the air density (ρ). So at different altitudes, the air density varies. In this case, where T/ρ and specific fuel consumption is constant and the engine control settings is fixed, the expression to find the range is can be altered by using the substitution method of equation 2.53 into equation 2.51 to obtain

$$R = \frac{1}{C_T} \sqrt{\frac{T}{S} \frac{2}{\rho} \frac{C_L^2}{C_D^3}} \ln \frac{W_1}{W_2} \quad (2.55)$$

Where maximum range requires maximum (C_L^2/C_D^3) when flying at different altitudes at a given airspeed and engine setting.

2.4 Turning Performance

Turning performance is one of the performance parameters in an aircraft. Basically, turning performance is an aircraft capability to make a turn by calculating a few parameters. The parameters that affect turning performance include the rate of turn, load factor, speed at turn, bank angle, radius of turn. In turn conditions, the aircraft lift value must match the weight. Other than that, must also correspond to the centrifugal force that occurs during the aircraft moving on a circular path.

2.4.1 Governing Equations

In coordinated turn we have the special conditions that the inward centripetal force required to pull to aircraft toward the center of the turn is accomplished by the horizontal component of the lift and that both the resultant aerodynamic force ($R + T$) and the vector sum of the weight and the outward centrifugal force ($W + C$) are in the plane of symmetry of the aircraft.

$$T - D - W \sin \gamma = 0 \quad (2.56)$$

$$W \cos \gamma \sin \mu - \cos \mu = 0 \quad (2.57)$$

$$-L + W \cos \gamma \cos \mu + C \sin \mu = 0 \quad (2.58)$$

Rather than the conventional air-path axis system used for symmetric flight, it is more convenient to employ for turning flight an additional axis system with axes X_t , Y_t , and Z_t . With the origin of the system at the center of gravity of the aircraft, the X_t -axis coincides with the X_a -axis. The Y_t -axis lies in the horizontal plane along the radius of curvature. The Z_t -axis lies in the vertical plane and is perpendicular to both the X_t and Y_t axes (Ruijgrok, 2009).

$$T - D - W \sin \gamma = 0 \quad (2.59)$$

$$L \sin \mu - C = 0 \quad (2.60)$$

$$-L \cos \mu + W \cos \gamma = 0 \quad (2.61)$$

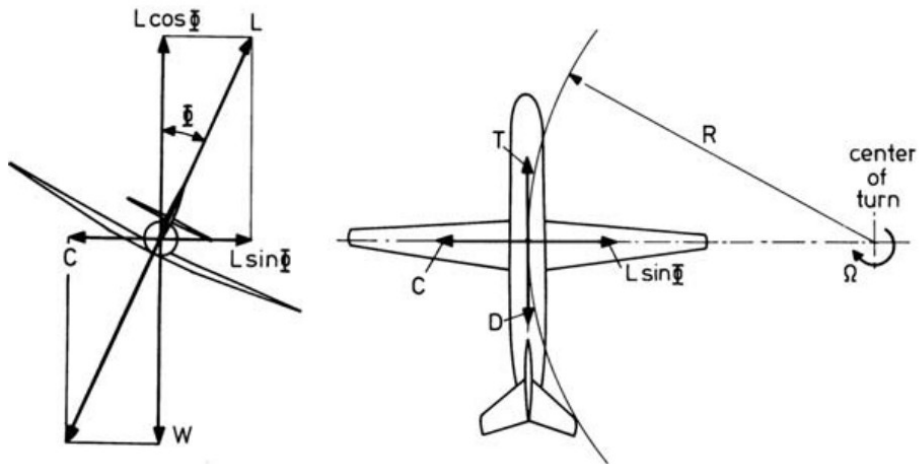


FIGURE 2.10: True banked turn of a aircraft during steady level flight

As shown on figure 2.10, In examining the instantaneous flight condition in a coordinated turn, it is customary to assume level flight ($\gamma = 0$) since the resulting

performance in level turning flight can be used to represent the performance in all normal climbing and descending turns (M. H. Sadraey, 2017) The aerodynamic angle of roll is equal to the bank angle ($\mu=\phi$). Furthermore, the centrifugal force can be distinguished as:

$$C = \frac{W V^2}{g R} \quad (2.62)$$

Where g is the acceleration of gravity ($g = 9.81\text{m/s}^2$) and R is the radius of turn.

For steady level turning flight, the governing equations can be simplified as

$$T - D = 0 \quad (2.63)$$

$$L \sin \phi - \frac{W V^2}{g R} = 0 \quad (2.64)$$

$$-L \cos \phi + W = 0 \quad (2.65)$$

Using the substitution method from the relationship of lift and drag

$$L = C_L \frac{1}{2} \rho V^2 S \quad (2.66)$$

$$D = C_D \frac{1}{2} \rho V^2 S \quad (2.67)$$

When substituting into equation 2.63 up to and equation 2.65, the equations can be altered to

$$T = C_D \frac{1}{2} \rho V^2 S \quad (2.68)$$

$$\frac{W V^2}{g R} = C_L \frac{1}{2} \rho V^2 S \sin \phi \quad (2.69)$$

$$W = C_L \frac{1}{2} \rho V^2 S \cos \phi \quad (2.70)$$

variables: α , V , Γ , R and ϕ so that the flight condition is determined by two control variables. In the next section we will express the various performance items in terms of angle of attack (C_L and C_D), and the angle of bank ϕ (Ruijgrok, 2009).

2.4.2 Performance in a Coordinated Turn Equations

In the event of a constant altitude turn, the airspeed can be obtained by the following equation

$$V = \sqrt{\frac{W}{S} \frac{2}{\rho} \frac{1}{\cos\phi}} \quad (2.71)$$

The drag during turning can be obtained by the following equation

$$D = W \frac{C_D}{C_L} \frac{1}{\cos\phi} \quad (2.72)$$

The power required to perform a turn can be distinguished by multiplying the drag and velocity to form the following equation. However, the power required gets limited by the power available of the target drone. Power available itself is the thrust multiplied by the velocity of the target drone.

$$P_r = DV = W \sqrt{\frac{W}{S} \frac{2}{\rho} \frac{C_D^3}{C_L^2} \frac{1}{\cos^3\phi}} \quad (2.73)$$

Figure 2.11 illustrates how turning radius can be determined (Ruijgrok, 2009). The equation to find the radius of turn can be distinguished from equation 2.69 and equation 2.70 as

$$R = \frac{W}{S} \frac{1}{g} \frac{1}{C_L} \frac{1}{\sin\phi} \quad (2.74)$$

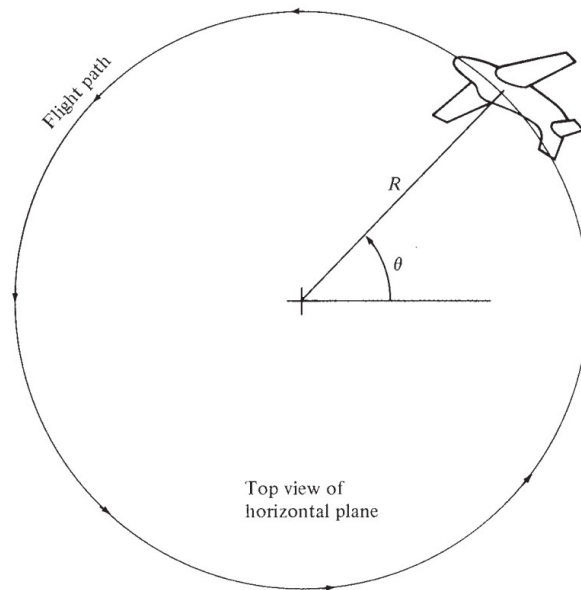


FIGURE 2.11: Determining the turning radius of an aircraft.

and

$$R = \frac{V^2}{g \tan \phi} \quad (2.75)$$

These equations represents that the radius of turn will be smaller when the bank angle or the load factor is larger, also when the airspeed during a turn is smaller.

The rate at which an aircraft turns can be distinguished from equation 2.74 and 2.75 into the following equation

$$\Omega = \frac{V}{R} = \frac{g \tan \phi}{V} \quad (2.76)$$

Rate of turn are expressed in terms of number of degrees the aircraft changes heading in one second.

From equation 2.76, it can be distinguished that the time needed to execute a 180° turn (π radians) is given by

$$T_\pi = \frac{\pi}{\Omega} = \frac{\pi V}{g \tan \phi} \quad (2.77)$$

The lower the airspeed, the smaller the bank angle required for a desired turning time T_π

Equations of V , D , Pr , R , ω , and T_π can be expressed with regards to bank angle or load factor. The load factor portrays the changes inversely as the cosine of the bank angle. The load factor (n) can be determined from the following equation:

$$n = \frac{L}{W} = \frac{1}{\cos \phi} \quad (2.78)$$

The angle of bank is the angle of roll at which the aircraft is making a turn while the load factor is the thrust to weight ratio of the target drone. Both the values of bank angle and load factor can be used when finding the turning performance. V , D , Pr , R , Ω , and T_π can be rewritten respectively with regards to load factor as follows:

$$V = \sqrt{\frac{nW}{S} \frac{2}{\rho} \frac{1}{C_L}} \quad (2.79)$$

$$D = nW \frac{C_D}{C_L} \quad (2.80)$$

$$Pr = nW \sqrt{\frac{nW}{S} \frac{2}{\rho} \frac{C_D^2}{C_L^3}} \quad (2.81)$$

$$R = \frac{W}{S} \frac{2}{\rho} \frac{1}{g C_L} \frac{n}{\sqrt{(n^2) - 1}} = \frac{V^2}{g \sqrt{(n^2) - 1}} \quad (2.82)$$

$$\Omega = g \frac{\sqrt{(n^2) - 1}}{V} \quad (2.83)$$

$$T_\pi = \frac{\pi V}{g \sqrt{n^2 - 1}} \quad (2.84)$$

CHAPTER 3

RESEARCH METHODOLOGY

The methodology of this research comprises of 8 steps where it will be used to fabricate chapter 4 of this thesis. Figure 3.1 shows the pathway that needs to be precisely done in order to successfully complete this research. The main steps can be elaborated in the following subsections.

3.1 Conceptual Design and Preliminary Sizing

From the conceptual design phase, the mission profile and the design requirements of the target drone were set by carrying out a benchmark study. The mean values from the benchmark study was used as a reference in order to pick out different configurations that would be short-listed depending on the design factor. The chosen configuration defines the body type, wing type, wing position, engine position, canard, tail, fuel tank and capacity, braking system, and landing gear that would determine the shape of the target drone. The type of airfoil, material, engine, electrical components, and payload were also selected.

Using the data obtained from the benchmark study, the preliminary sizing for the target drone can be determined. Once finalized, a draft design is assembled by utilizing SolidEdge as the project's CAD software. By choosing the material of the target drone, Solidedge allows users to estimate the weight, center of gravity, and aerodynamic center of the target drone.

From the aircraft weight, sizing, and engine specification, the variables obtained from this process that would help obtain results for this research are listed as follows:

- Length
- Wingspan

PERFORMANCE REVIEW AND ANALYSIS OF GUAV-190417 TARGET DRONE:
CRUISING AND TURNING

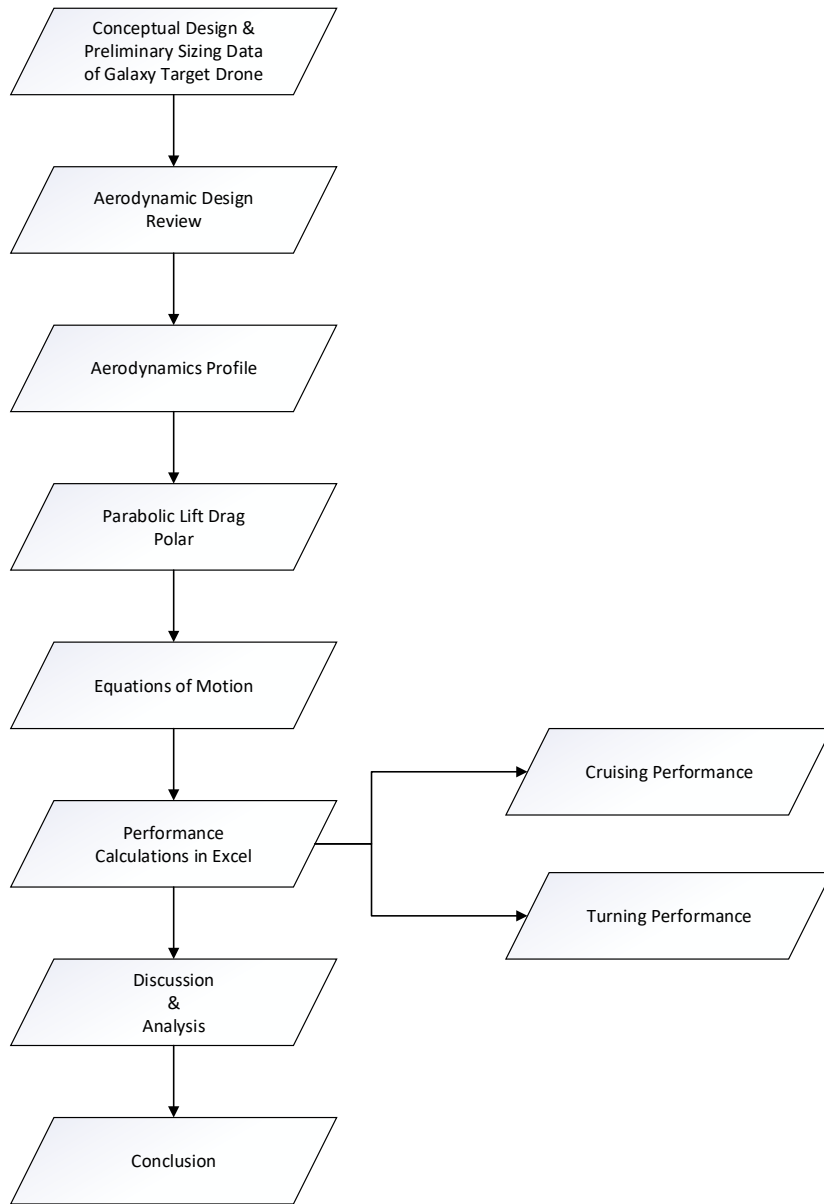


FIGURE 3.1: Step-by-step process to determine the performance of GUAV-190417

- Chord at tip and root
- Swept angle
- MTOW

- Empty weight
- Mach
- Viscosity
- Thrust
- Mass fuel rate
- Specific fuel consumption

3.2 Aerodynamics Review

In order to determine the aerodynamic characteristics, the CAD file with the correct weight and sizing was formatted into .stl and gets uploaded to OpenFOAM v8.0 software where the viscous pressure of the target drone gets simulated. The outcome of the CFD simulation would be the lift and drag coefficients.

Using simpleFOAM solver, the laminar simulations gets carried out using steady state scheme. The model gets resized 0.4x of its original size to be able to undergo the available pre-processing functions in OpenFOAM.

The computational dimensions of the model which consists of the length, height, and width of the computational domain are set to 1.7, 1.0, and 0.5 in x, y, z; respectively; in non-dimensional values.

Taking the time constraint into consideration; since the target drone is symmetrical in the x-y plane; only half of the flow around the target drone gets simulated to reduce computational time. A slight increase in pressure drag is expected since the front nozzle of the nozzle is defined as a closed structure.

As seen in figure 3.2, by using SnappyHexMesh, the mesh gets generated to discretized the computational domain (Greenshields, 2018). The total meshes in the simulation are shown as follows:

In order to portray the flow in zero angle of attack $\alpha=0$, as part of the boundary conditions, the stream wise velocity was set to 100m non dimensional vales while other components such as transverse and span verse velocities are set to zero.

The target drone model gets defined as no-slip wall boundary condition, so that $\frac{d\phi}{dn} \neq 0$.

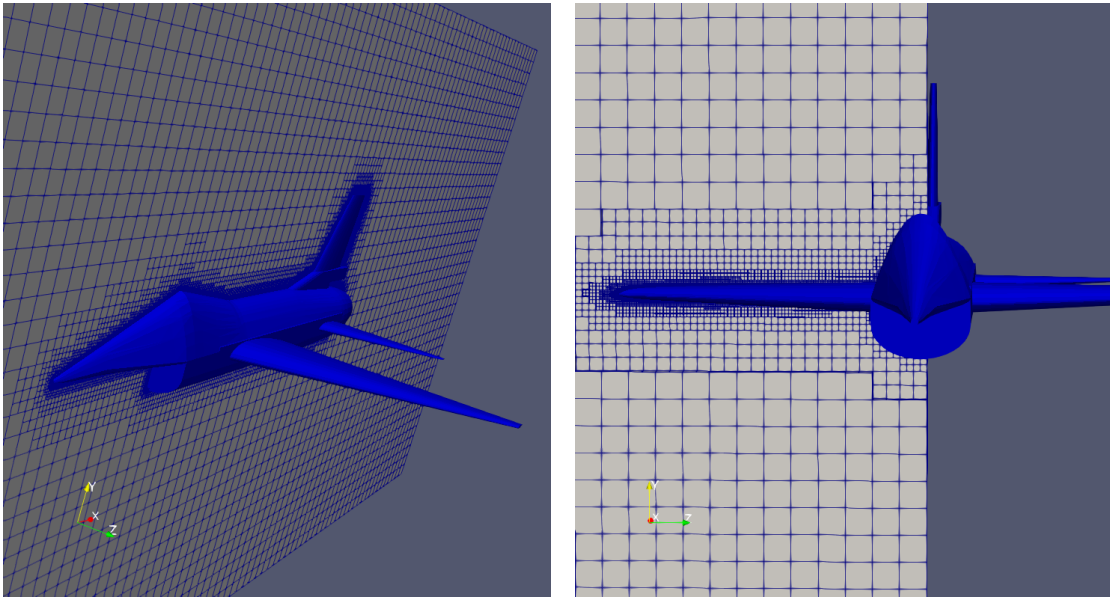


FIGURE 3.2: Mesh topology of computational domain.

Mesh elements	Number
Hexahedral	3 647 081
Prism	195 682
Polyhera	672 859
Total meshes:	4 517 622

TABLE 3.1: Meshes used in the simulation

Analyzing using Paraview software, the overall computation time of 5000 iterations is ~ 26 hours. 16 GB of RAM and 4 processors were utilized in this process. The convergence was achieved after 2000 iterations.

3.3 Aerodynamics Profile Estimation

The aerodynamics profile of the target drone can be obtained through aerodynamics calculations using variables available from the airfoil characteristics and the wing dimensions (McCormick, 1994). These variables are used in equations 2.24, 2.19, 2.11, and 2.8 respectively to obtain:

- Lift coefficient (C_L)

- Drag coefficient (C_D)
- Reynolds number (Re)
- Aspect ratio (AR)

To obtain the lift and drag coefficients, the following factors must be applied:

- Aircraft should be in equilibrium condition
- Angle of attack must be 0 ($\alpha=0$)
- Aircraft should be at sea-level

By following the listed factors, the lift and drag along with the drag and thrust are set to have equal values.

3.4 Parabolic Lift Drag Polar Estimation

The outcome of the aerodynamics profile such as the lift, drag, and zero drag coefficients are used as variables to calculate the parabolic lift drag polar. By inserting the lift, drag, and zero drag coefficients into equations 2.66, 2.67, and 2.36 respectively would result in finding the values of:

- $C_L/C_{D_{\max}}$
- $C_L^3/C_{D_{\max}}^2$
- $C_L/C_{D_{\max}}^2$

3.5 Performance Estimation Using Excel

In this section, like shown in figure 3.3, the performance requirements are mentioned in order to carry out the performance analysis. The equations mentioned are prepared in excel ready to be computed in different conditions using different variables. The values obtained from different conditions will then be analyzed.

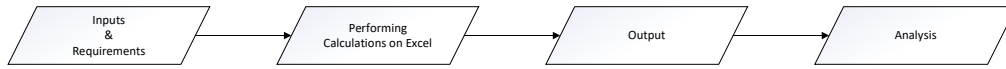


FIGURE 3.3: Performance Calculation Overview.

3.5.1 Cruising Performance Estimation

For cruising performance, The flight profile is steady straight non side-slipping flight. The following parameters are required to estimate the range and endurance of an aircraft:

- Constant angle of attack
- Constant altitude
- Constant velocity
- Constant specific fuel consumption
- Fixed engine settings
- Zero side-slip

In this section, the range and endurance of the target drone is calculated using weight fractions ranging from 1.0 up to 1.3 with a step of 0.05. The calculations for range are calculates at heights from 0m up to 4000m with a step of 1000m.

Equations 2.51 and 2.52 would respectively result in finding the values of the range and endurance at sea level. By varying the weight fraction from a minimum of 1 and a maximum of 2, the range and endurance of the target drone can be graphically compared. Equations 2.53 and 2.54 would respectively result in the finding the values of the thrust and the velocity required to calculate the range and endurance at different altitudes. In this case, equations 2.55 and 2.52 would result in finding the values of the range and endurance at different altitudes.

3.5.2 Turning Performance Estimation

For turning performance, the flight profile is non side-slipping banked turn. The following parameters are required to estimate the range and endurance of an aircraft:

- Constant angle of attack
- Constant altitude
- Constant velocity
- Zero side-slip

In this section, the turning radius, rate of turn, and $T\pi$ of the target drone is calculated using two different variables:

1. Bank angle (ϕ)
2. Load factor (n)

There are two types of calculations that needs to be carried out:

1. Turning performance using different bank angles at sea level
2. Turning performance using different load factor at different altitudes

Equations 2.71, 2.72, 2.73, 2.74, and 2.75 would respectively result in finding the values of the velocity, drag, power required, radius of turn, rate of turn, and the time required to make a 180° turn at sea level. The results of turning radius and the rate of turn can be graphically compared with respect to its bank angle.

Meanwhile, equation 2.78 is used to find the load factor which will be applied into equations 2.79, 2.80, 2.81, 2.82, 2.83, and 2.84 to respectively find the values of the velocity, drag, power required, radius of turn, rate of turn, and the time required to make a 180° turn. These values can be subjected in different altitude by altering the value of the air density in equations 2.79, 2.81, and 2.82.

CHAPTER 4

RESULTS AND DISCUSSIONS

4.1 Aerodynamics Analysis Using OpenFOAM

The result of lift coefficient from OpenFOAM simulation can be presumed to be almost similar to the results obtained using manual calculation by referring to $C_L\alpha$ graph. The comparison between both result are shown in table 4.1.

Lift coefficient	Value
OpenFoam simulation	0.3826
Manual estimation	0.3529

TABLE 4.1: C_L comparison between OpenFOAM and manual estimation.

The drag coefficient was not able to be obtained using OpenFOAM simulation since the available drag polar is only for the airfoil/ wing, the parasite drag of the whole target drone can not be estimated. Therefore, using simulation, the parasite drag for the whole target drone is obtained $C_{D_0} \equiv 0.0469$.

From Figure 4.1, the warm colors presents the areas at which pressure is highest while the cooler colors is where pressure is lowest. The areas at which the pressure is high are the areas that can be seen from the front such as the nose, the nozzle, and the front of the wings. Meanwhile, the areas that can be seen from the top such as the upper surface of the fuselage and the wing experience less pressure.

The graph portrayed on figure 4.2 describes the relationship between the coefficient of drag (C_D) and the coefficient of lift (C_L) of the target drone. It can be clearly seen that as the C_L increases, the C_D also increases accordingly.

The graph portrayed on figure 4.3 illustrates how the coefficient of drag (C_D) value varies depending on the number of iterations performed. It can be clearly

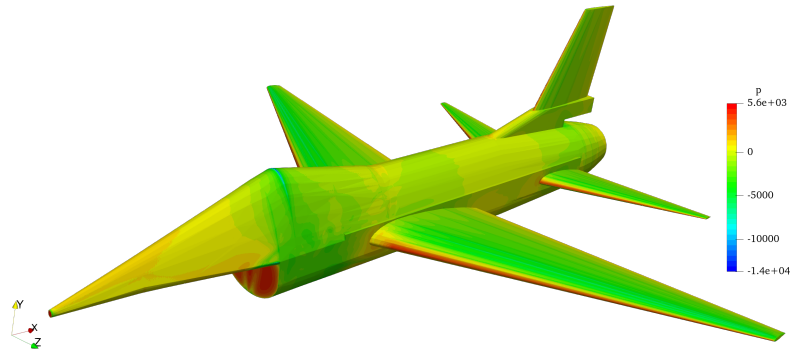


FIGURE 4.1: OpenFOAM results: Pressure distribution.

seen that the C_D value increases in a fluctuating movement. The value of the C_D is seen to remain steadily around the values of 0.035 up to 0.04.

4.2 Cruising Performance

Generally, target drone cruise at fixed flight levels that are usually the most fuel efficient. When the weight of the target drone decreases and the atmospheric conditions alter, the optimal cruise altitude will also change. To calculate the cruising requirements, there are few matters that should be acknowledged, such as thrust and drag forces, conditions of the atmosphere, specific fuel consumption, and the mass of the target drone. Given that the GUAV-190417 deals with the steady parameters of the flight, limiting the scope of the model to constant altitude and angle of attack (α) is the solution. The focus of the model is to describe the common and maximum values of range and endurance of the target drone.

By utilizing this flight profile, it is suitable for long range mission profiles such as patrol, surveillance, and without a doubt, target practice as it improves the flight endurance of an target drone. However, it is not so fuel efficient. For an target drone cruising at a constant angle of attack (α) and constant altitude, the velocity of the target drone is constantly adjusted as the weight decreases due to fuel emission to achieve the range and endurance required.

The results obtained on figure 4.4 and figure 4.5 shows the range and endurance that were estimated using different weight fractions. The weight fraction is set up

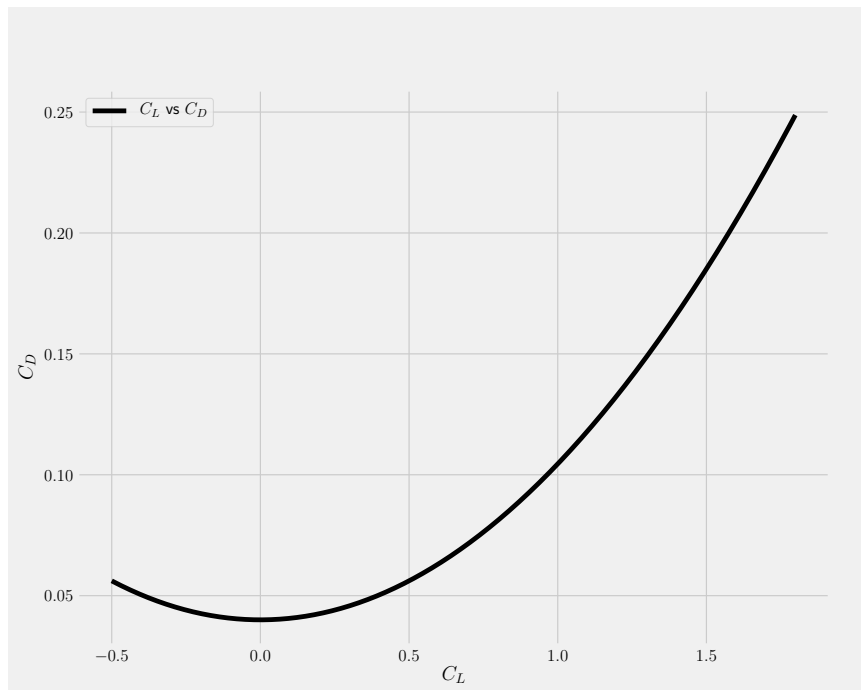


FIGURE 4.2: OpenFOAM results: relationship between C_L and C_D .

from a minimum of 1.0 and a maximum of 1.3, with a difference of 0.05. It can be seen that the range and the endurance of the target drone increases along with the increasing weight fraction.

On figure 4.4, the range is subjected at different altitudes; starting from 0 m (sea-level) up to 4000 m. It is clearly shown that with increasing altitude, the range increases respectively. The maximum range at sea level using weight fraction 1.25 is 215 km. However, on figure 4.5, as air density is not a factor of endurance, the endurance remains constant at different altitudes. Referring to the graph provided, it is clearly shown that the endurance of the target drone increases along with the increasing of the weight fraction. The maximum endurance obtained was 90 minutes.

4.3 Turning Performance

The objective of this section is to estimate performance parameters that are related to the individual turns of the GUAV-190417. These parameters include the power

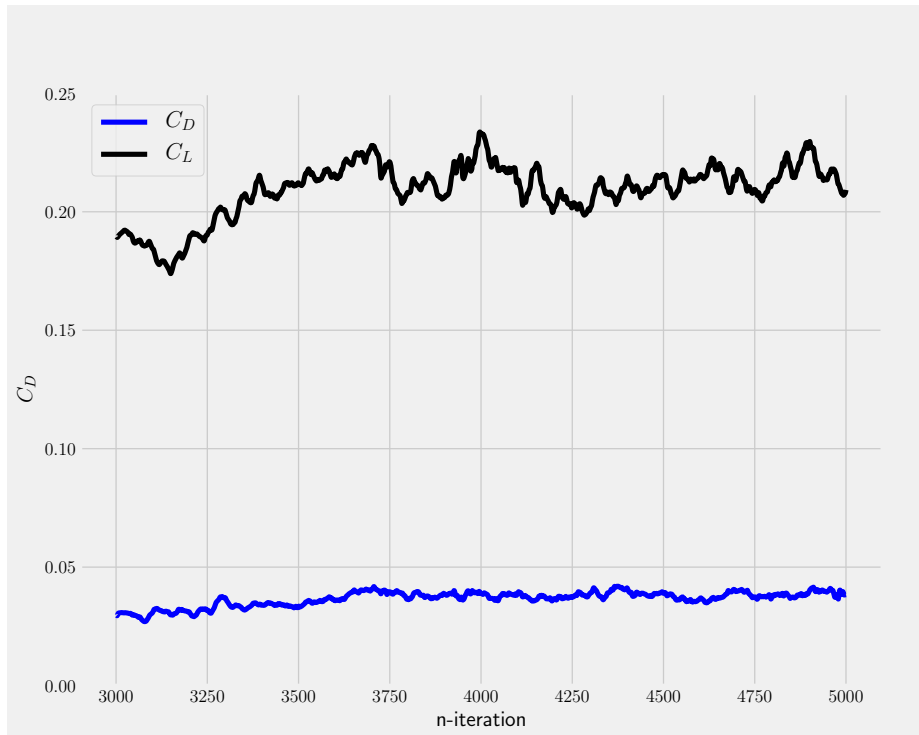


FIGURE 4.3: OpenFOAM results: C_D at different iterations.

required to make a turn, turn radius, turn rate, and the time required to make a 180° at different bank angles or load factors. Elements such as weather phenomena or non standard atmosphere conditions which influences the turning performance of an target drone are not taken into consideration.

So, at angle of attack (α) = 0° , for a perfect turn (no skidding), it can be distinguished that the velocity and the corresponding drag could be calculated to find the power required. The velocity and the corresponding drag could further be used to find the radius and rate of turn of the target drone. The total lift of the target drone needs to be increased in order to maintain a steady flight considering the rolling of the target drone. As the lift of the target drone is increased, this results to an increase in the drag of the target drone as well as the thrust of the target drone.

The drag and power required curves due to banking and turning can be distinguished by taking the flight condition and the angle of bank of the target drone into consideration. At sea level (I.S.A), for a target drone with a thrust of 200 N turning at constant angle of attack, it can be seen from figure 4.6 and 4.7 that

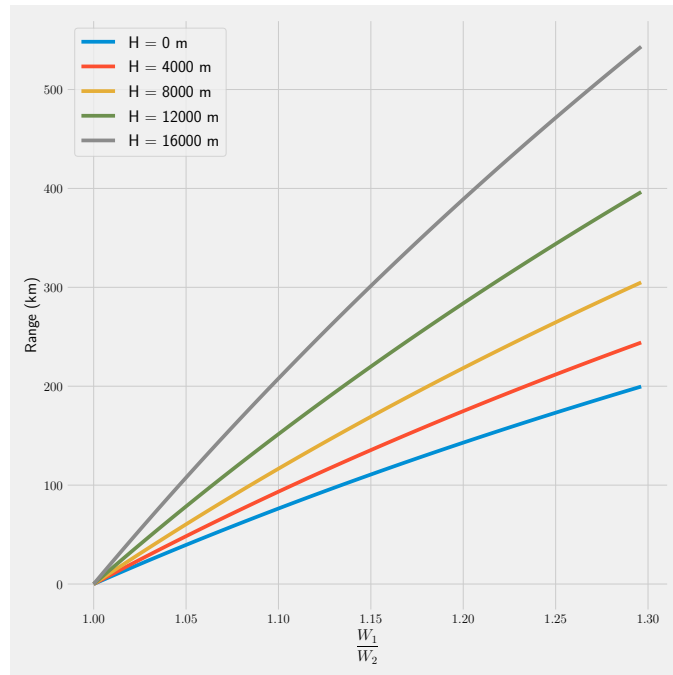


FIGURE 4.4: Range of GUAV-190417 using different weight fractions at different altitudes

the values of airspeed, drag, and power required increases with respect to a greater bank angle. The power available is the factor that limits the target drone and distinguish the most extreme turning performance in terms of bank angle. The

Compressibility drag may occur for a target drone that flies at a subsonic level, meaning that the lift and drag coefficients must be distinguished from the lift-drag polar for the turning flight airspeed at each flight velocity.

Figure 4.8, 4.9, 4.10, and 4.11 portrays the affects of radius of turn, banking angle, load factor, and T_π at 180° as functions of the airspeed of the target drone at different altitudes. The altitude was varied from 0 m (sea-level), 3000 m, and 8000 m at constant engine control settings. The maximum altitude that can be reached by the target drone has been distinguished at 15200 m. Beyond 15200m, the power available will not be sufficient to perform the turn. The trend obtained was that the turning performance strongly declines with increasing altitude. The maximum load factor decreases with altitude due to the decrease of air density and thrust at higher altitudes. The altitude gives similar affects on the values of turning radius and T_π . Oppositely, the airspeed shows a gradual increase with respect to higher

PERFORMANCE REVIEW AND ANALYSIS OF GUAV-190417 TARGET DRONE:
CRUISING AND TURNING

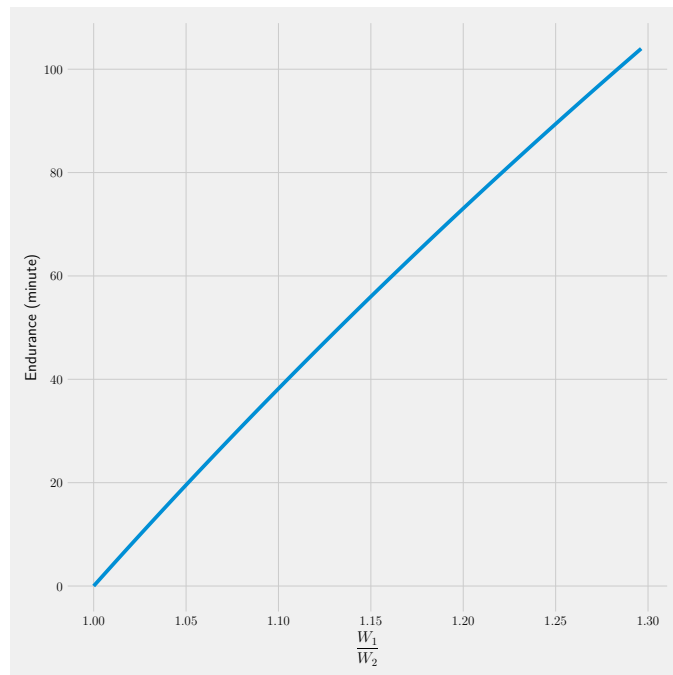


FIGURE 4.5: Endurance of GUAV-190417 using different weight fractions

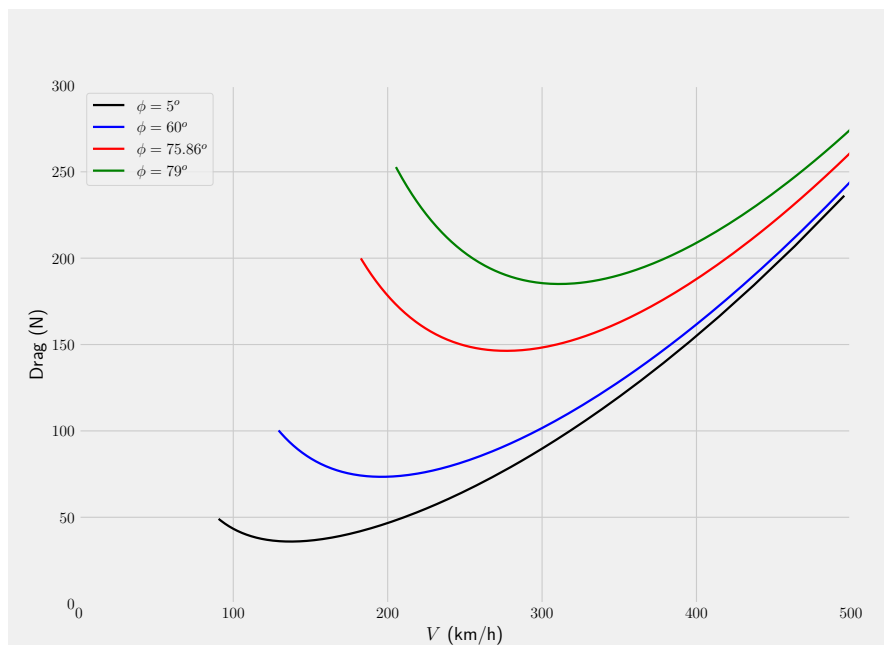


FIGURE 4.6: Drag at sea-level

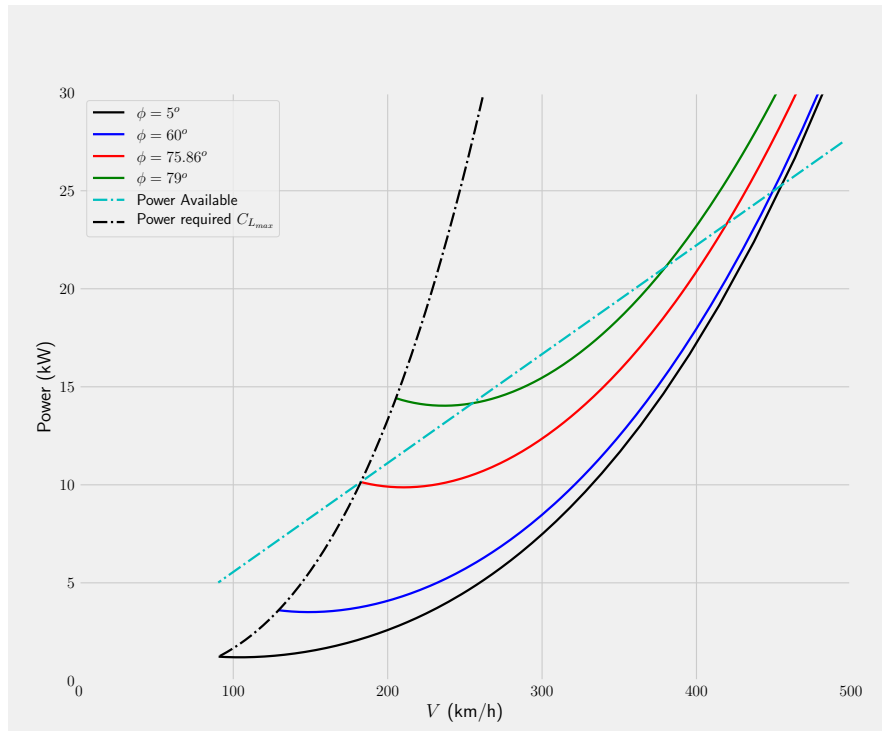


FIGURE 4.7: Power required at sea-level

altitude.

From figure 4.8, the minimum turning radius at 0m (sea-level) is 66.07 m at an airspeed of 185.00 km/h. Meanwhile, the turning radius at 15200 (maximum altitude) is 453.41m at an airspeed of 292.86 km/h.

From figure 4.9 and 4.10, the maximum bank angle at 0m (sea-level) that can be performed by the target drone is 80.96° at an airspeed of 306.64 km/h. Consequently, the value of the maximum load factor subjected to target drone is 6.36 at the same airspeed. At 15200 (maximum altitude), the maximum bank angle that can be performed by the target drone is 66.24° at 477.08 km/h. On the contrary, the value of the maximum load factor subjected to target drone is 2.48 at the same airspeed.

From figure 4.11, the minimum turning time to perform a 180° (T_π) turn at 0m (sea-level) is 3.73 s at an airspeed of 223.37 km/h. Meanwhile, minimum turning time to perform a 180° turn at 15200m (maximum altitude) is 16.19 s at an airspeed of 353.07 km/h.

PERFORMANCE REVIEW AND ANALYSIS OF GUAV-190417 TARGET DRONE:
CRUISING AND TURNING

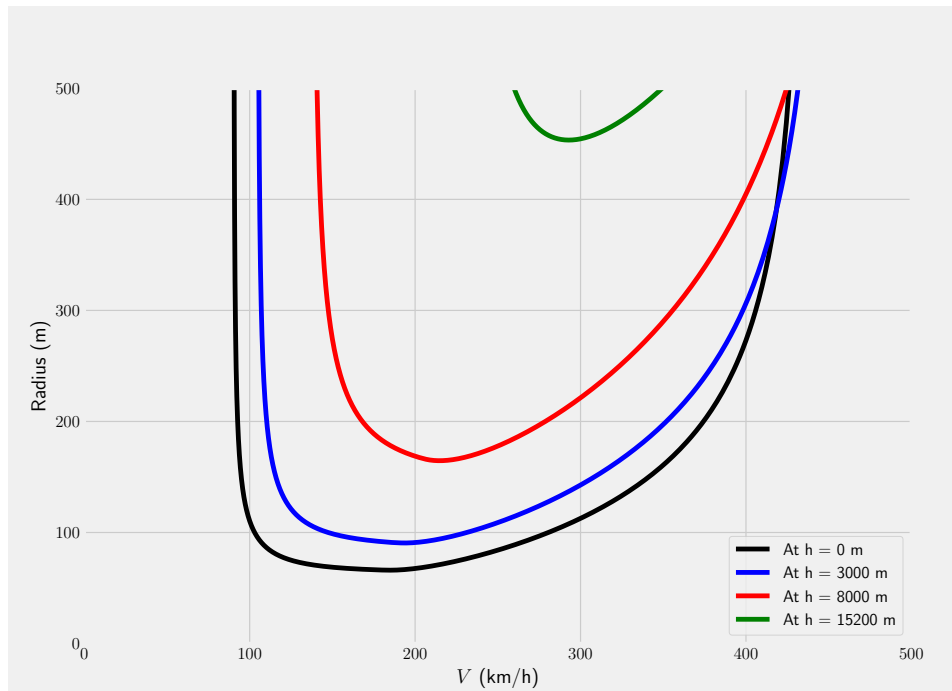


FIGURE 4.8: Radius of turn at different altitudes

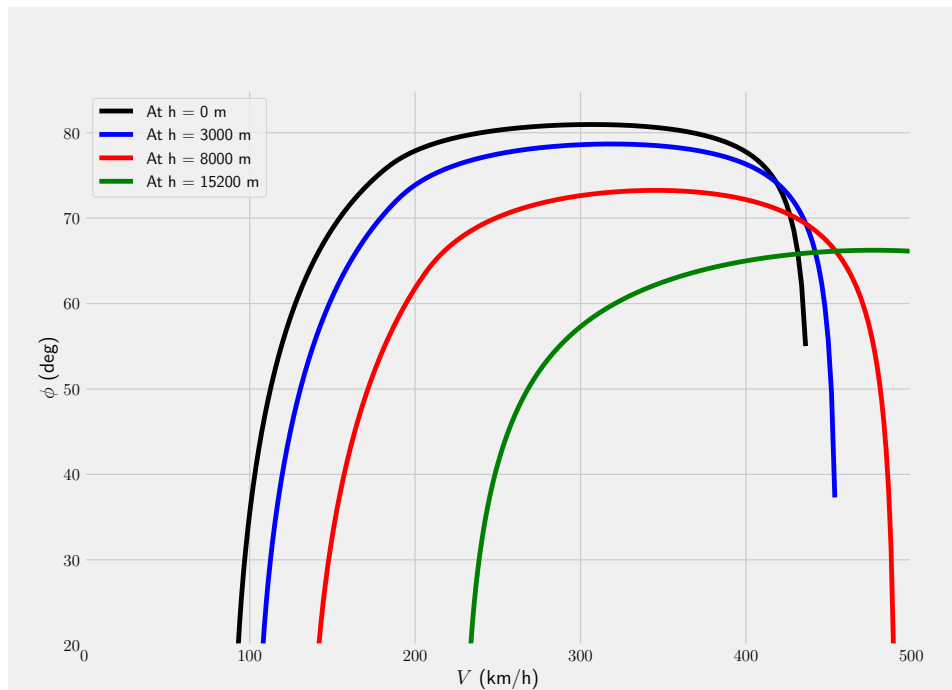


FIGURE 4.9: Load factor and the airspeed at different altitudes

PERFORMANCE REVIEW AND ANALYSIS OF GUAV-190417 TARGET DRONE:
CRUISING AND TURNING

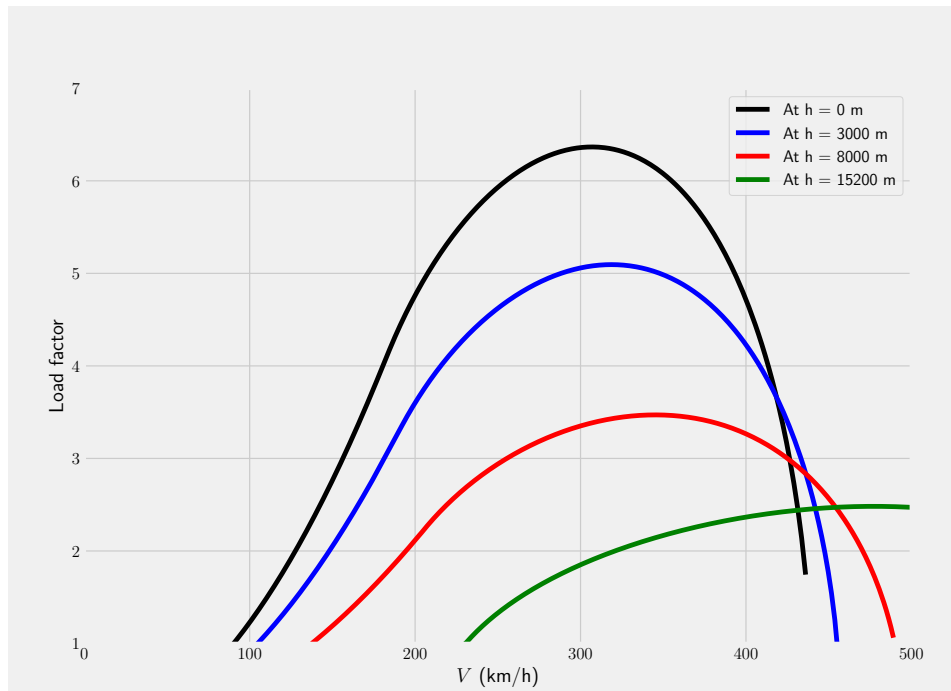


FIGURE 4.10: Load factor and the airspeed at different altitudes

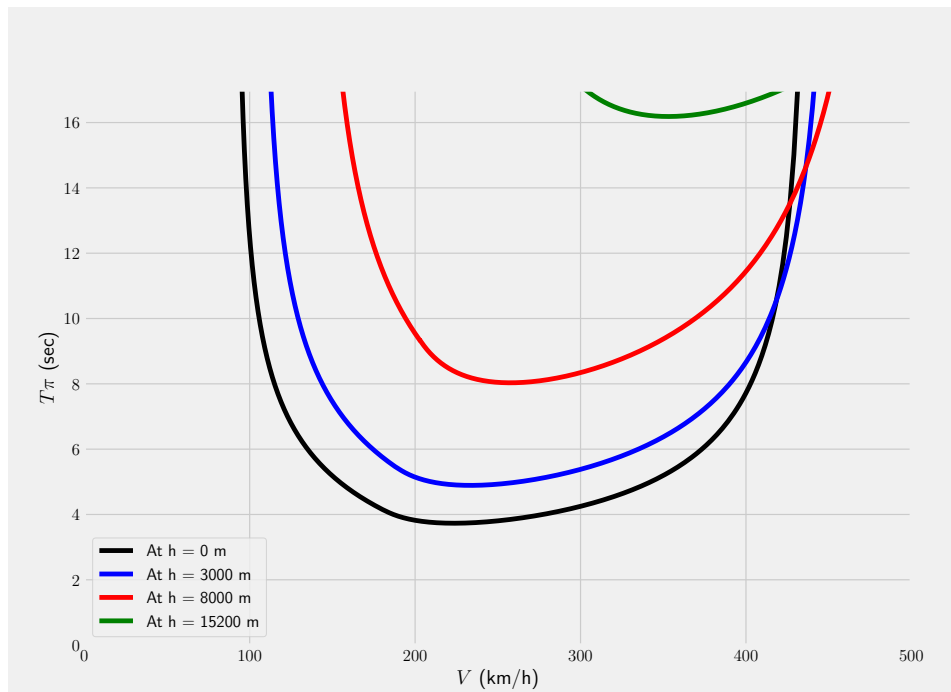


FIGURE 4.11: Time required to make a 180° turn at different altitudes

CHAPTER 5

SUMMARY, CONCLUSION, RECOMMENDATION

5.1 Conclusion

The sole objective of this research is to analyze the GUAV-190417 design to review whether if it is eligible to move on to the next phase of design, which is detailed design, prototype manufacturing, and flight test. The determination whether if the design is qualified or not can be done by comparing its performance analysis to the initial mission profile of the GUAV-190417, specifically in the cruising and turning segments of flight. From the results obtained from this research analysis, it can be concluded that:

1. Aerodynamics Performance:

- The use of OpenFOAM software for this research analysis has proven that the coefficient of lift (C_L) value that was calculated manually by referring to the $C_{L\alpha}$ graph is similar to the value obtained from the simulation using OpenFOAM. The analysis includes the calculation of the coefficient of lift (C_L) at 0° . By simulating it in OpenFOAM software, the result of the C_L value is found at 0.3826, whereas by manual estimation, the result of the C_L value is found at 0.3529. The result for the parasite drag value is obtained at $C_D = 0.0469$. The simulation results also shows that the drag coefficient varies as the square of the lift coefficient.

2. Cruising Performance:

- The flight profile for maximum range and endurance requires the target drone to be in a cruise configuration. The total range and endurance

are functions of the weight of the target drone, which is changing continuously as fuel is consumed. Hence, a weight factor is used when calculating the the range and endurance of the target drone to take into account the weight loss due to fuel burnt to reach the cruising segment of flight. The specific fuel consumption makes a significant impact to the cruising performance.

- When calculated at different altitudes, the trend achieved was that the higher the altitude, a longer range for the target drone can be obtained while the endurance remain constant as the air density at different altitudes does not impact the endurance of the flight.
- The cruising performance analysis resulted with the values of range and endurance of 215km/h and 90 minutes respectively.

3. Turning Performance:

- The target drone can reach a maximum altitude of 15 200m. the radius and the time required to make a 180° turn is 453.41m and 16.19s respectively. The maximum bank angle and load factor is 80.96° and 6.36 respectively at an airspeed of 223.37km/h. At sea level, the radius and the time required to make a 180° turn is 66.07m and 3.73s respectively.
- The turn at any given bank angle is proportional to the square of the initial velocity. However, at unaccelerated flight where the initial airspeed remains constant, the bigger the bank angle will decrease the turning radius. The relationship achieved were the opposite of those observed in rate of turn, where the bigger the initial speed decreases the rate of turn and the bigger the bank angle also increases the rate of turn. The maneuverability of the target drone gets enhanced as the flight altitude of the target drone is decreased.

Overall, the aerodynamics calculations were done as precise as possible as it has been proven by the OpenFOAM simulation. The range and endurance acquired exceeded the author's expectations. However, some adjustments can be made to optimize the performance of the target drone. The turning performance

has sufficed the mission profile of the target drone as it has proven to have a good maneuverability.

5.2 Recommendation

1. A better lift drag polar results can be achieved by optimizing the configuration of the target drone, especially the wing shape and size. The aspect ratio can be optimized as it affects the lift and drag coefficients.
2. The endurance can be improved by optimizing the weight of the target drone. It can be observed that the higher the weight increases the drag due to induced and profile drag. A bigger thrust is needed to equalize the drag, which results in a greater fuel flow, which reduces the endurance. Hence why is it recommended to optimize the weight of the target drone as not only it will increase the endurance but also the range of the target drone.
3. The range and endurance can also be increased by using an optimized engine, which has a better specific fuel consumption. This will all result to a bigger weight fraction, which will impact the weight and endurance drastically.
4. For further continuation of this project, once the performance analysis are all done, there are other analysis to be made before moving on to the detailed design, prototype manufacturing, and flight test phase such as FEM analysis and stability and control analysis.

References

- Anderson Jr, J. D. (2010). *Fundamentals of aerodynamics*. Chennai, India: Tata McGraw-Hill Education.
- Greenshields, C. J. (2018). Openfoam user guide version 6. *The OpenFOAM Foundation*.
- Mccormick. (1994). *Aerodynamics, aeronautics, and flight mechanics*. John Wiley & Sons. Retrieved from https://www.ebook.de/de/product/3635471/mccormick_aerodynamics_aeronautics_and_flight_mechanics.html
- McGhee, R. J. (1980). *Low-speed aerodynamic characteristics of a 17-percent-thick medium speed airfoil designed for general aviation applications*. National Aeronautics and Space Administration, Scientific and Technical .
- Raymer, D. (2012). *Aircraft design: a conceptual approach*. Reston, VA: American Institute of Aeronautics and Astronautics, Inc.
- Roskam, J. (1986). *Airplane design*. Lawrence, Kan: DARcorporation.
- Ruijgrok, G. (2009). *Elements of airplane performance*. Place of publication not identified: VSSD.
- Sadraey, M. (2017). *Unmanned aircraft design : a review of fundamentals*. San Rafael, California: Morgan & Claypool Publishers.
- Sadraey, M. H. (2012). *Aircraft design: A systems engineering approach*. John Wiley & Sons. Retrieved from https://www.ebook.de/de/product/18698777/sadraey_mohammad_h_sadraey_aircraft_design.html
- Sadraey, M. H. (2017). *Aircraft performance: an engineering approach*. Boca Raton: CRC Press.
- Valavanis, K. P. (2014). *Handbook of unmanned aerial vehicles*. SPRINGER NATURE. Retrieved from https://www.ebook.de/de/product/11883304/handbook_of_unmanned_aerial_vehicles.html
- Yong, J. Y. H. (2021). *Performance review and analysis of guav-190417 target drone: Airfield, symmetric climbing, and gliding*.

Appendices

Turnitin Report

PERFORMANCE REVIEW AND ANALYSIS OF GUAV-190417 TARGET DRONE: CRUISING AND TURNING

ORIGINALITY REPORT

6%

SIMILARITY INDEX

4%

INTERNET SOURCES

2%

PUBLICATIONS

2%

STUDENT PAPERS

PRIMARY SOURCES

1

repository.tudelft.nl

Internet Source

1%

2

dynlab.mpe.nus.edu.sg

Internet Source

1%

3

Submitted to Middle East Technical University

Student Paper

<1%

4

www.airtarget.se

Internet Source

<1%

5

www.nextor.org

Internet Source

<1%

6

en.wikipedia.org

Internet Source

<1%

7

Submitted to Technische Universiteit Delft

Student Paper

<1%

8

John D. Anderson. "Aeronautics", Wiley, 2003

Publication

<1%

9

Submitted to Institute Of Applied Technology

Student Paper

<1%

10

Submitted to Emirates Aviation College,
Aerospace & Academic Studies

Student Paper

<1%

11

ijltet.org

Internet Source

<1%

12

Trevor M. Young. "Mechanics of Maneuvering
Flight", Wiley, 2017

Publication

<1%

13

www.ijert.org

Internet Source

<1%

14

Peng Nian, Bifeng Song, Jianlin Xuan, Wenqing
Yang, Yuanbo Dong. "A Wind Tunnel
Experimental Study on the Flexible Flapping
Wing With an Attached Airfoil to the Root", IEEE
Access, 2019

Publication

<1%

15

www.absoluteastronomy.com

Internet Source

<1%

16

Submitted to University of Hertfordshire

Student Paper

<1%

17

Submitted to University of Wales Swansea

Student Paper

<1%

buaya-instrument.com

18	Internet Source	<1%
19	sites.google.com Internet Source	<1%
20	Submitted to University Tun Hussein Onn Malaysia Student Paper	<1%
21	Torenbeek. "Aeroplane Performance", Flight Physics, 2009 Publication	<1%
22	Submitted to Rutgers University, New Brunswick Student Paper	<1%
23	Submitted to Asian Institute of Technology Student Paper	<1%
24	Submitted to University of Sheffield Student Paper	<1%
25	cmup.fc.up.pt Internet Source	<1%
26	Saarlas. "Maneuvering Flight", Aircraft Performance, 12/12/2006 Publication	<1%
27	www.ijee.ieefoundation.org Internet Source	<1%
28	Florent Le Bras, Tarek Hamel, Robert Mahony,	<1%

Christian Barat, Julien Thadasack. "Approach maneuvers for autonomous landing using visual servo control", IEEE Transactions on Aerospace and Electronic Systems, 2014

Publication

29

www.coursehero.com

Internet Source

<1%

30

www.irbnet.de

Internet Source

<1%

31

Lin, C.F.. "Optimum three-dimensional flight of a supersonic aircraft", Applied Mathematical Modelling, 198204

Publication

<1%

32

Ernst Heinrich Hirschel, Claus Weiland. "Selected Aerothermodynamic Design Problems of Hypersonic Flight Vehicles", Springer Science and Business Media LLC, 2009

Publication

<1%

33

Osamu Kobayashi. "Definition System and Criteria Related to the Static Stability of Airplanes. (First Report). Definition System, Static Flight Speed Stability, and Static Angle of Attack Stability.", TRANSACTIONS OF THE JAPAN SOCIETY FOR AERONAUTICAL AND SPACE SCIENCES, 2002

Publication

<1%

hal.upmc.fr

Exclude quotes Off

Exclude matches Off

Exclude bibliography Off



Curriculum Vitae

Basic Information	
Name	Raihan Syauqi
Place of Birth	Serang, Banten
Date of Birth	10, 05, 2000
Address	BSD City, South Tangerang, Banten, Indonesia

Year	Education
2017 - present	International University Liaison Indonesia
2014 - 2017	The Cambridge School - Doha, Qatar (High School)

Year	Courses
2020	Basic Python
2019	Basic Latex
2018	SolidWorks
2018	3D Printing
2017	IELTS

Year	Seminars & Workshops
2020	MRO 4.0
2019	Aircraft Maintenance
2018	Industry 4.0
2018	Aircraft Flight Testing
2018	Smart Materials

Year	Work Experiences
2019	Sriwijaya Air - Maintenance planning and control
